

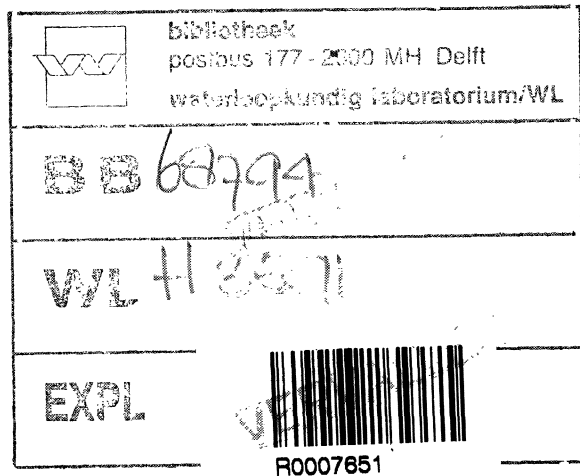
Prepared for:

Rijkswaterstaat, National Institute for Coastal and
Marine Management (RIKZ)

Boundary conditions for a 2D Boussinesq-type wave model

AFTENBESLUIT

January 2000



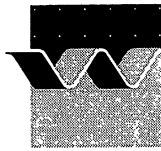
Boundary conditions for a 2D Boussinesq-type wave model

M.J.A. Borsboom, J. Groeneweg, N. Doorn, M.R.A. van Gent

January 2000



wl | delft hydraulics



CLIENT: Rijkswaterstaat, National Institute for Coastal and Marine Management (RIKZ)

TITLE: Boundary conditions for a 2D Boussinesq-type wave model

ABSTRACT: Boundary conditions are developed for an existing 2D Boussinesq-type wave model. This wave model was designed for accurate modelling of wave propagation in coastal regions and harbours. The method and the implementation of the developed module for open and closed wave boundaries is validated using three sets of physical model tests. Also a method for partly reflecting boundaries is developed such that the reflection characteristics of beaches and coastal structures can be modelled. The main conclusions are that the performance of the boundary conditions is very good. Although the method can be seen as a state-of-the-art technique, further improvements can be obtained for situations with irregular wave trains as incident waves.

SAMENVATTING: De randafhandeling voor Boussinesq-type golfmodellen is bestudeerd in dit project. Het (abstract in Dutch) toegepaste Boussinesq-type golfmodel is ontwikkeld voor golfmodellering in kust- en havengebieden. Voor dit type modellen is de afhandeling van de zeewaartse en landwaardse randen van belang zodat de randen niet tot ongewenste verstoringen van het golfveld in het te modelleren gebied leiden. In dit project zijn zeewaartse randen (volledig open) en landwaartse randen (volledig gesloten) ontwikkeld en geïmplementeerd, en vervolgens gevalideerd aan de hand van een drietal datasets uit laboratorium metingen. Daarnaast is ook een methode ontwikkeld voor gedeeltelijk reflecterende randen zodat de reflectie-eigenschappen van bijvoorbeeld stranden en zeeweringen adequaat gemodelleerd kunnen worden. De belangrijkste conclusie is dat de ontwikkelde methode zeer goed werkt. Als vervolgonderzoek wordt onder andere aanbevolen om de methode nog verder te optimaliseren voor toepassingen met onregelmatige golftreinen als inkomende golven.

REFERENCES: Contract RKZ-741 within the framework ZEESPIEG,
Offer MCI05670/H3581/MvG/im, dd. 21-7-1999

REV.	ORIGINATOR	DATE	REMARKS	REVIEW	APPROVED BY
0	Borsboom et.al.	Nov. 1999	Draft	M.R.A. van Gent	W.M.K. Tilmans
1	Borsboom et.al.	Jan. 2000	Final	M.R.A. van Gent	W.M.K. Tilmans

KEYWORDS

Numerical wave model

Boundary conditions

Boussinesq model

Absorbing boundaries

Partly-reflecting boundaries

STATUS

PRELIMINARY

DRAFT

FINAL

PROJECT IDENTIFICATION: H3581

Contents

List of Figures

List of Symbols

1	Introduction.....	1–1
2	Description of the 2D Boussinesq-type wave model.....	2–1
2.1	Main features of the computational model.....	2–1
2.2	The 2D Boussinesq-type model equations	2–2
3	Boundary conditions.....	3–1
3.1	Analysis of the 2D Boussinesq-type equations	3–1
3.2	Seaward boundary: weakly reflecting	3–8
3.3	Landward boundary: partially reflecting or fully reflecting.....	3–11
3.4	The details.....	3–14
4	Validation of boundary conditions	4–1
4.1	Performance of weakly reflecting wave boundaries.....	4–1
4.2	Performance of model with 1D shoal	4–4
4.3	Performance of model with 2D shoal	4–6
4.4	Discussion of results.....	4–8
5	Conclusions and recommendations.....	5–1

References

Figures

List of Figures

In text:

- 1 Boundary with local co-ordinate system and local variables
- 2 Definition sketch of domain used in reflection tests over horizontal bottom
- 3 Bottom geometry of Beji and Battjes' (1993) submerged bar in a wave flume and location of the wave gauges
- 4 Bottom geometry of Berkhoff et al.'s (1982) 2D shoal

In Appendix Figures:

- F1a Reflection errors for wave amplitude $a = 1.0\text{cm}$, wave period $T = 1.5\text{s}$ and angle of incidence $\theta = 0^\circ$ at $t = 7.04\text{s}$
- F1b Reflection errors for wave amplitude $a = 1.0\text{cm}$, wave period $T = 1.5\text{s}$ and angle of incidence $\theta = 20^\circ$ at $t = 7.68\text{s}$
- F1c Reflection errors for wave amplitude $a = 1.0\text{cm}$, wave period $T = 1.5\text{s}$ and angle of incidence $\theta = 45^\circ$ at $t = 10.24\text{s}$
- F2 Water level elevation computed in Ω_2 and in Ω_3 for waves with $a = 1.0\text{cm}$, $T = 1.5\text{s}$ and $\theta = 20^\circ$
- F3 Reflection errors for wave amplitude $a = 5.0\text{cm}$, wave period $T = 1.5\text{s}$ and angle of incidence $\theta = 20^\circ$ at $t = 7.68\text{s}$
- F4a Reflection errors for wave amplitude $a = 1.0\text{cm}$, wave period $T = 1.0\text{s}$ and angle of incidence $\theta = 20^\circ$ at $t = 5.1\text{s}$
- F4b Reflection errors for wave amplitude $a = 1.0\text{cm}$, wave period $T = 8.0\text{s}$ and angle of incidence $\theta = 20^\circ$ at $t = 40.0\text{s}$
- F5a Comparison of time series of surface elevation at stations 1-6 for measurement condition A (Dingemans, 1994)
- F5b Comparison of time series of surface elevation at stations 7-11 for measurement condition A (Dingemans, 1994)
- F6 Reflection errors at $t_n = 50.5\text{s}$ obtained with present analysis and long wave assumption
- F7 Computed values for c_{Bous}^- at left and right boundary
- F8a Comparison of numerical results and experimental data for wave heights on measuring transects 1, 2 and 5 of Berkhoff et al. (1982)
- F8b Comparison of numerical results and experimental data for wave heights on measuring transects 6 and 7 of Berkhoff et al. (1982)

List of Symbols

Roman letters:

a	: wave amplitude (m)
c_{Bous}	: phase speed (wave celerity) as modelled by Boussinesq-type equations (m/s)
g	: gravitational acceleration constant (m^2/s)
h	: water depth with respect to reference level (m)
H	: total water depth (m)
$k, \mathbf{k}, \mathbf{k}^\perp$: wave number, wave number vector, orthogonal rotation of that vector (1/m)
L	: length scale (m)
n	: normal space co-ordinate (m)
p_b	: pressure divided by density at bottom (m^2/s^2)
P	: depth-integrated pressure divided by density (m^3/s^2)
P'_b	: modified pressure divided by density at bottom (tensor) (m^2/s^2)
q, \mathbf{q}	: depth-integrated velocity, depth-integrated velocity vector (m^2/s)
Q	: amplitude of depth-integrated velocity per wave component (m^2/s)
r	: reflection coefficient (-)
s	: tangential space co-ordinate (m)
t	: time (s)
T	: wave period (s)
$\bar{u}, \bar{\mathbf{u}}$: depth-averaged velocity, depth-averaged velocity vector (m/s)
\mathbf{x}	: space co-ordinate vector (m)
Z	: amplitude of water level per wave component (m)

Greek letters:

α, β	: model parameters (-)
δ	: small coefficient (-)
ε	: measure of non-linear effects (-)
ζ	: water level with respect to reference level (m)
λ	: wave length (m)
θ	: wave angle with respect to normal direction (rad)
φ	: phase shift (rad)
μ	: measure of linear dispersion (-)
μ_s	: measure of linear shoaling (-)
ω	: wave frequency (1/s)
$\omega_{\text{expl}},$	
ω_{impl}	: correction coefficients (-)
ω_r	: underrelaxation coefficient (-)

Superscripts, subscripts:

\sim	:	auxiliary variable
$'$:	modified variable
0	:	variable related to convection
$-,+ \quad$:	outgoing, incoming wave component
bc	:	variable at boundary
giv	:	variable prescribed at boundary
i	:	index of wave component
n	:	normal component
p	:	projected value
s	:	tangential component
typ	:	typical value

I Introduction

Boussinesq-type wave models are in principle suitable to model wave propagation in coastal regions and harbours. Especially for the wave propagation of short waves, where non-linear effects play an important role, this type of model can be adequately applied and provide valuable information on the wave field which cannot accurately be obtained from many other types of models (e.g., time series of surfaces and velocities in shallow regions).

The 2D Boussinesq-type model applied here is a model developed to obtain an accuracy as good as possible within limited computing times. Besides a proper balance between accuracy and computing time also a proper balance was found between the accuracy of the mathematical description and accuracy of the numerical implementation. The mathematical description and the numerical source code of the 2D Boussinesq-type model applied here was developed at WL | DELFT HYDRAULICS under the name TRITON. The main features of this model of which a few are unique within the wide range of existing Boussinesq-type models, are discussed in the following chapter.

The present project concerns the development, the implementation and the validation of a module to treat wave boundary conditions in the above mentioned 2D Boussinesq-type model. This module is developed as generic as possible such that it in principle can also be used for a series of other types of shallow-water wave equation models. The boundaries concern open boundaries as seaward boundaries (weakly reflecting boundaries) and closed boundaries as landward boundaries (fully reflecting boundaries). The code is validated by comparisons with results from three series of physical model tests.

Also a method for a partially reflecting wave boundary is developed, although not implemented and validated, so that the reflection can be modelled as function of the wave frequency. This yields boundaries where for instance long waves can be fully reflected while the short waves at the same time are only reflected partly. In contrast to almost all available other methods, this is a unique method which models the physical behaviour of for instance beaches and coastal structures where long waves are reflected to a much higher degree than short waves.

The main features of the applied 2D Boussinesq-type wave model are described in Chapter 2. In Chapter 3 the theoretical background and the implementation of the boundary conditions is described. The validation of the model with the implemented boundary conditions is described in Chapter 4. Chapter 5 provides an overview of the main conclusions with respect to the boundary conditions and suggestions for further investigations on this subject are given.

2 Description of the 2D Boussinesq-type wave model

2.1 Main features of the computational model

A number of parameters is important in describing the properties of Boussinesq-type wave models: typical water depth h_{typ} , typical wave amplitude a_{typ} , typical wave number k_{typ} , and typical horizontal length L_{typ} over which changes in bottom level occur. They are combined to the non-dimensional numbers:

- $\epsilon = a_{typ} / h_{typ}$, indicating the relative importance of non-linear effects,
- $\mu = k_{typ} h_{typ}$, indicating the relative importance of linear dispersion,
- $\mu_s = 1/(k_{typ} L_{typ})$, indicating the relative importance of linear shoaling.

The Boussinesq-type equations that are considered in this report model these effects to $O(\epsilon\mu^2, \mu_s^2\mu^4, \mu^6)$. So only non-linear long-wave effects are included, and the modelling of shoaling over steep bottoms is limited. On the other hand, the modelling of linear dispersion as well as linear shoaling over moderate slopes has been improved and describes also the behaviour of fairly short waves.

This (order of) accuracy is typical of Boussinesq-type models of several years ago (Madsen and Sørensen, 1992; Nwogu, 1993). Since then, authors have worked on extending either the linear accuracy (Schäffer and Madsen, 1995; Dingemans and Merckelbach, 1997) or the non-linear accuracy (Wei et al., 1995), or both (Madsen and Schäffer, 1998; Gobbi and Kirby, 1999). The number of variations that exists within these modelling frameworks is staggering (Dingemans, 1997; Borsboom, 1998).

The main issue for practical purposes is to construct a Boussinesq-type model with a good balance between its different modelling qualities, tailored to the requirements of the applications it is intended for. For example, for the large amplitude waves we are particularly interested in, it is useless to improve the linear accuracy without enhancing the non-linear modelling terms (Wei et al., 1995; Gobbi and Kirby, 1999). The improvement of both leads to highly accurate, but also highly complicated Boussinesq-type equations (Madsen and Schäffer, 1998; Gobbi and Kirby, 1999). These models perform indeed better in test applications like the one described in Section 4.2. On the other hand, they are considerably more expensive to implement and more expensive to run. Also, a number of important aspects related to their practical use has not yet been addressed, such as weakly reflecting and partially reflecting boundary conditions, and the extension with a breaking wave model. Gobbi and Kirby (1999) even avoid the need for suitable boundary conditions entirely, by applying a source term inside the domain to generate the wave signal in combination with sponge layers in the outer regions to absorb all spurious reflected waves.

For these reasons it has been decided to start the present development with a Boussinesq-type formulation having a what may nowadays be called ‘standard’ accuracy, and to develop suitable boundary procedures and a breaking wave model first. However, we have used the freedom in design to develop a model that has a number of unique properties:

1. formulation is totally independent of the (arbitrary) vertical reference level for bottom topography and water elevation,
2. dispersion and shoaling are modelled in a very compact way,
3. both mass and momentum are conserved.

The first property ensures an easy and transparent use of the model, while the second property makes the model fairly efficient (Borsboom, 1998). The third property has been developed recently from the Boussinesq-type equations presented in Borsboom (1998) that conserve only mass. In the new formulation the physical properties of mass conservation and momentum conservation are both retained. The conservation of momentum makes it very easy to extend the model with, e.g., a breaking wave model that only dissipates wave energy but does not alter the total amount of momentum; momentum is only redistributed.

Notice that properties 1 and 3 put a number of physical constraints on the design of the model. In principle it is allowed to modify a Boussinesq-type model arbitrarily within its order of accuracy. The present approach limits this design freedom and excludes the higher-order modifications that do not make sense physically. We anticipate that this improves the general performance of the model, especially at the limits of its range of applicability. Some level of arbitrariness is however unavoidable, and has currently been used to simplify the equations as much as possible. Obviously, this use of freedom of design may require re-evaluation in the future. It is worth mentioning that the derivation of the model equations has shown that property 2 and 3 lead in fact to roughly the same result, which explains why it is possible to combine both in the same formulation.

Some experiments have shown that the new formulation is indeed an improvement; the new model behaves more stable and is easier to use than its predecessor described in Borsboom (1998). It has been verified that higher-order extensions of the model are possible without having to sacrifice any of its desirable features. Details of the model can be found in the next section. Its derivation will be published in Borsboom et al. (2000).

2.2 The 2D Boussinesq-type model equations

We present the equations of the new 2D Boussinesq-type model in a form that allows easy identification of the physical meaning of the different terms:

$$\frac{\partial H}{\partial t} + \nabla \cdot \mathbf{q} = 0 , \quad (2.1)$$

$$\frac{\partial \mathbf{q}}{\partial t} + \nabla \cdot (\bar{\mathbf{u}}\mathbf{q}) + \nabla P = p_b \nabla h , \quad (2.2)$$

$$\text{with: } P = g \frac{\tilde{H}^2}{2}, \quad p_b = g \left(\frac{3\tilde{H}}{2} - \frac{H}{2} + \frac{H}{4} \nabla H \cdot \nabla \zeta \right), \quad (2.3)$$

$$\begin{aligned} \text{and: } & \tilde{H} - \alpha H^2 \nabla^2 \tilde{H} - \beta H \nabla h \cdot \nabla \tilde{H} = H - \left(\alpha - \frac{1}{3} \right) H^2 \nabla^2 H - \left(\beta - \frac{1}{2} \right) H \nabla h \cdot \nabla H + \\ & - \frac{1}{2} (\nabla h \cdot \nabla h) H - \frac{1}{3} (H \nabla^2 h) H. \end{aligned} \quad (2.4)$$

The unknowns in these equations are total water depth H and depth-integrated velocity vector \mathbf{q} ; the water depth with respect to some arbitrary reference level h is given and describes the specified bathymetry. From these variables the water elevation with respect to the reference level $\zeta = H - h$ and the depth-averaged velocity vector $\bar{\mathbf{u}} = \mathbf{q}/H$ are obtained. Auxiliary variable \tilde{H} is a function of H , defined implicitly by (2.4). This equation realises a [2,2] Padé approximation of $O(\mu^6)$ of linear dispersion and the first order effect of linear shoaling that can be adjusted by respectively α and β . The value of these parameters should be 0.4 or slightly lower (Borsboom, 1998).

Auxiliary variables P and p_b have been introduced because of their physical meaning. From the conservative form of momentum equation (2.2) it can be seen immediately that P and p_b must represent respectively the depth-integrated pressure and the pressure at the bottom, both divided by the density that is assumed constant. The former appears in (2.2) as its gradient, while the latter appears in a source term that is scaled with bottom slope ∇h . The gradient term is in conservative form, expressing the conservation of horizontal pressure forces inside the fluid. The source term is non-conservative and expresses the horizontal pressure reaction force at the bottom that is proportional to the slope of the bottom. Both are exactly as one would expect from physical principles.

Notice that for $|\nabla H| \ll 1$ we have $\tilde{H} \rightarrow H$ and therefore $P \rightarrow g H^2/2$ and $p_b \rightarrow gH$. This is the shallow-water limit ($\mu \ll 1$), with P and p_b equal to respectively the depth-integrated hydrostatic pressure and the hydrostatic pressure at the bottom (the weight of the water column), divided by the density. In other words, the deviation of P and p_b from these hydrostatic values indicates the non-hydrostatic effects introduced by the propagation of shorter waves as modelled by the Boussinesq-type equations.

Another interesting limit is obtained by considering $|\nabla \zeta| \ll 1$ and hence $|\bar{\mathbf{u}}| \ll \sqrt{gH}$. In this linear limit where the convection term in (2.2) vanishes ($\varepsilon \ll 1$), P and p_b depend only on \tilde{H} and H showing that the linear behaviour of the model is essentially determined by equation (2.4). So this is the equation to be modified if the linear range of applicability of the model is to be extended.

Concerning the non-linear extension of the model, it has been shown in Borsboom (1998) that the convection term in (2.2) is accurate up to $O(\varepsilon\mu^4)$. So terms of $O(\varepsilon\mu^2)$ (as said

before, effects of this order are *not* included properly in the above model equations) can only be higher-order non-linear pressure corrections. This has been confirmed by a preliminary investigation, where a velocity-dependent correction of $O(\epsilon\mu^2)$ was derived for P . This term appears to be direction-independent, i.e., it behaves indeed like a pressure component.

The previous paragraphs show that the present Boussinesq-type formulation is suitable for future higher-order extensions, but also indicate that the model allows easy verification of the physical nature of the different modelling terms. The latter is a significant advantage over other, far more complex Boussinesq-type models that hardly permit a physical interpretation. Furthermore, the compact form of the present equations has simplified considerably its numerical implementation.

The design of suitable boundary conditions for the equations (2.1) and (2.2) will be the subject of the next chapter. However, also dispersion equation (2.4) requires boundary conditions. Ideally, these boundary conditions should be obtained from a detailed analysis of the three-dimensional velocity field that is implicitly described by the Boussinesq-type equations, reconstructing the velocity profile in vertical direction in a way that is consistent with the applied dispersion approximation. Such an analysis is very tedious and has never been applied to our knowledge, although Wei and Kirby (1995) present a boundary condition obtained by means of a strongly simplified version of this procedure. In view of these difficulties, we have applied at the boundaries:

$$\tilde{H} - \alpha H^2 \frac{\partial^2 \tilde{H}}{\partial s^2} - 0.8H \frac{\partial \tilde{H}}{\partial n} = H - \left(\alpha - \frac{1}{3} \right) H^2 \frac{\partial^2 H}{\partial s^2} - 0.3H \frac{\partial H}{\partial n}, \quad (2.5)$$

with s the co-ordinate tangential to the boundary and n the co-ordinate normal to the boundary pointing inward. This equation has been obtained from (2.4) that for a uniform bottom ($\nabla h = 0$) can be written as, neglecting higher-order non-linear terms:

$$(\mathbf{e} + \sqrt{\alpha} H \nabla) \cdot (\mathbf{e} - \sqrt{\alpha} H \nabla) \tilde{H} = (\mathbf{e} + \sqrt{\alpha - 1/3} H \nabla) \cdot (\mathbf{e} - \sqrt{\alpha - 1/3} H \nabla) H, \quad (2.6)$$

with \mathbf{e} the unit normal vector pointing inward. Since the boundary condition for elliptic equation (2.4) can at most have first derivatives in normal direction, we have to omit at the boundary the normal derivative in the first part of the differential operator in the left- and right-hand side of (2.6):

$$\tilde{H} - \alpha H^2 \frac{\partial^2 \tilde{H}}{\partial s^2} - \sqrt{\alpha} H \frac{\partial \tilde{H}}{\partial n} = H - \left(\alpha - \frac{1}{3} \right) H^2 \frac{\partial^2 H}{\partial s^2} - \sqrt{\alpha - 1/3} H \frac{\partial H}{\partial n}.$$

This is equation (2.5), except for the fact that typical values of $\sqrt{\alpha}$ and $\sqrt{\alpha - 1/3}$ are about 0.63 and 0.25 respectively. Experiments have shown that if the wave direction is normal to the boundary, better results are obtained with slightly larger values. This is because the definition of vector \mathbf{e} is not unique. The difficulties that we have encountered in the applications with waves propagating at a certain angle suggest that \mathbf{e} should probably depend on

the dominant wave direction. Unfortunately, omitting terms in (2.6) to construct a boundary condition for (2.4) will always lead to a condition that will introduce some combination of phase and amplitude errors near the boundaries. A totally different and undoubtedly considerably more complex approach is required to avoid this, but this lies outside the scope of the present project.

Note that in principle we could equally well have neglected the normal derivative in the second part of the differential operator in the left- and right-hand side of (2.6), but that would lead to a discretisation that is not diagonally dominant anymore. As for the discretisation of (2.1), (2.2) and (2.4) and their boundary conditions, a conservative second-order accurate finite-difference method has been used which retains the conservation properties of the model.

3 Boundary conditions

3.1 Analysis of the 2D Boussinesq-type equations

The reflection properties of boundary conditions for the system of equations (2.1)–(2.4) depend entirely on the transport phenomena described by this hyperbolic system. We will therefore begin this chapter with an analysis of its properties. It is then more convenient to write (2.1) and (2.2) in the quasi-linear form:

$$\begin{aligned} \frac{\partial \zeta}{\partial t} + \nabla \cdot \mathbf{q} &= 0, \\ \frac{\partial \mathbf{q}}{\partial t} + (\bar{\mathbf{u}} \cdot \nabla) \mathbf{q} + \bar{\mathbf{u}}(\nabla \cdot \mathbf{q}) - (\bar{\mathbf{u}} \bar{\mathbf{u}}^T) \nabla \zeta + g \tilde{H} \nabla \tilde{\zeta} &= \mathbf{P}'_b \nabla h. \end{aligned} \quad (3.1)$$

These equations have been obtained by the substitution of $\partial H / \partial t = \partial \zeta / \partial t$, $\nabla H = \nabla \zeta + \nabla h$ and $\nabla \tilde{H} = \nabla \tilde{\zeta} + \nabla h$, introducing the auxiliary variable $\tilde{\zeta} = \tilde{H} - h$. This leaves the terms $-(\bar{\mathbf{u}} \bar{\mathbf{u}}^T) \nabla h$ and $g \tilde{H} \nabla h$ which have been added to the right-hand side. So we have (cf. (2.3)):

$$\mathbf{P}'_b = p_b \mathbf{I} + \bar{\mathbf{u}} \bar{\mathbf{u}}^T - g \tilde{H} \mathbf{I} = g \left(\frac{\tilde{H} - H}{2} + \frac{H}{4} \nabla H \cdot \nabla \zeta \right) \mathbf{I} + \bar{\mathbf{u}} \bar{\mathbf{u}}^T, \quad (3.2)$$

with \mathbf{I} the two-by-two identity matrix, i.e., \mathbf{P}'_b is a tensor, in contrast with p_b which is a scalar.

Notice that expression (3.2) includes some effects of $O(\varepsilon \mu^2)$. Effects of that order are outside the range of the model and therefore in essence ‘arbitrary’ (see Chapter 2). For example, the last term in the right-hand side of (3.2) may just as well be omitted, while the coefficient $\nabla H \cdot \nabla \zeta$ could be replaced by $\nabla \tilde{H} \cdot \nabla \zeta$ or even by $\nabla h \cdot \nabla \zeta$; such modifications are of $O(\varepsilon \mu^2)$ and hence do not alter the formal order of accuracy of the current Boussinesq-type model. It is clear however that they will have a noticeable effect on the actual performance of the model in applications with fairly short waves that are not small, but then we are also at the limit of the range of applicability of the model (the value of $\varepsilon \mu^2$ is not small anymore). We mention this here merely to elucidate some of the remarks made in Chapter 2.

We continue the analysis of the properties of (3.1) and consider the general situation of a curved boundary. To this end, we introduce the local co-ordinate system $\mathbf{x} = (n, s)^T$, with

co-ordinate n normal to the boundary pointing *inward* and co-ordinate s tangential to the boundary (see Figure 1). All variables will be formulated in this local reference system, so we have $\mathbf{q} = (q_n, q_s)^T$, $\bar{\mathbf{u}} = (\bar{u}_n, \bar{u}_s)^T$ and $\nabla = (\partial/\partial n, \partial/\partial s)^T$.

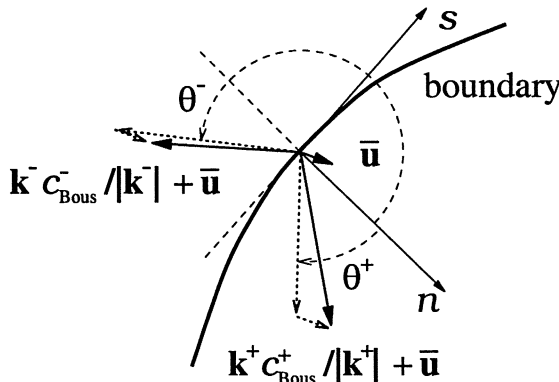


Figure 1: boundary with local co-ordinate system and local variables

We write the water level locally (i.e., in a small neighbourhood of the origin of the local co-ordinate system) as the sum of a number of wave components ζ_i , $i = 1, 2, \dots$, and a component that contains the remaining part of the solution (ζ_0 , pertaining to stationary and convection processes):

$$\zeta(\mathbf{x}, t) = \zeta_0(\mathbf{x}, t) + \sum_{i \geq 1} \zeta_i(\mathbf{x}, t) = \zeta_0(\mathbf{x}, t) + \sum_{i \geq 1} \operatorname{Re}(Z_i(\mathbf{x}, t) e^{i(\mathbf{k}_i(\mathbf{x}, t) \cdot \mathbf{x} - \omega_i(\mathbf{x}, t)t)}). \quad (3.3)$$

Notice that in Figure 1 only two wave components have been drawn: one incoming (\mathbf{k}^+) and one outgoing (\mathbf{k}^-). The meaning of the other variables in Figure 1 will be explained later.

Decomposition (3.3) is assumed to be such that the following conditions are satisfied:

$$\begin{aligned} \left| \frac{\partial \zeta_0}{\partial t} \right| &\ll \omega_{\min} \|Z_i\|, \quad i = 1, 2, \dots, \\ \left| \nabla Z_i \right| &\ll k_{\min} \|Z_i\|, \quad \left| \frac{\partial Z_i}{\partial t} \right| \ll \omega_{\min} \|Z_i\|, \quad i = 1, 2, \dots, \\ \left| \nabla \mathbf{k}_i \right| &\ll k_{\min} |\mathbf{k}_i|, \quad \left| \frac{\partial \mathbf{k}_i}{\partial t} \right| \ll \omega_{\min} |\mathbf{k}_i|, \quad i = 1, 2, \dots, \\ \left| \nabla \omega_i \right| &\ll k_{\min} \omega_i, \quad \left| \frac{\partial \omega_i}{\partial t} \right| \ll \omega_{\min} \omega_i, \quad i = 1, 2, \dots, \end{aligned} \quad (3.4)$$

with $k_{\min} = \min |\mathbf{k}_i|$ and $\omega_{\min} = \min \omega_i$ respectively the lowest wave number and the lowest frequency, and with $\| \cdot \|$ some suitable norm to measure the local size of the wave amplitudes Z_i .

The first condition of (3.4) is to ensure that ζ_0 contains no or at most only a negligible wave-like part, and specifies that convection should be small near the boundaries. This is no restriction since the Boussinesq-type equations form essentially a wave model and are not meant to serve as a flow model. It does not imply that the velocity as such needs to be small; it only means that the variations in space (if any) of the velocity and water level associated with convection should be roughly in equilibrium. That is, any gradients related to convection should be (almost) stationary and therefore balance each other.

The remaining conditions of (3.4) exclude large variations of the amplitudes Z_i , the wave numbers $k_i = |\mathbf{k}_i|$ and the frequencies ω_i in both time and space, and are satisfied when non-linear and shoaling effects are not excessively large. This is not a restriction either, since large non-linear and shoaling effects cannot be handled by the model anyway. Furthermore, the conditions (3.4) have to hold only near the boundaries, where convection, non-linearities and shoaling may be expected to be fairly small in general.

The idea behind decomposition (3.3) is to write any behaviour of the water level at a boundary locally as the sum of a very slowly varying component $\zeta_0(\mathbf{x}, t)$ and a (preferably small) number of wave-like components $\zeta_i(\mathbf{x}, t)$ that each have a smoothly and slowly varying amplitude $Z_i(\mathbf{x}, t)$ and a smoothly and slowly varying wave number vector and frequency $\mathbf{k}_i(\mathbf{x}, t)$ and $\omega_i(\mathbf{x}, t)$. We consider only positive frequencies ($\omega_i > 0$) so the wave number vectors $\mathbf{k}_i = (k_{n,i}, k_{s,i})^T$ indicate the direction of propagation of the wave-like components: incoming waves have $k_{n,i} > 0$ while outgoing waves are characterised by $k_{n,i} < 0$.

Inserting (3.3) in (2.4) we obtain, using (3.4) to neglect the terms involving space derivatives of Z_i and \mathbf{k}_i :

$$\zeta(\mathbf{x}, t) = \zeta_0 + \sum_{i \geq 1} \zeta_i \approx \tilde{\zeta}_0 + \sum_{i \geq 1} \frac{1 + \alpha(k_i H)^2}{1 + (\alpha - 1/3)(k_i H)^2} \tilde{\zeta}_i = \sum_{i \geq 0} \frac{g \tilde{H}}{c_{\text{Bous},i}^2} \tilde{\zeta}_i, \quad (3.5)$$

where we have neglected also all terms proportional to the bottom slope ∇h which at the boundary is assumed to be small. For $i \geq 1$, the $c_{\text{Bous},i}$ in this expression denote the Boussinesq approximation of the dispersive wave speed of each wave component i in (3.3), while for the convection component ($i = 0$) the long-wave celerity $c_{\text{Bous},0} = \sqrt{g \tilde{H}}$ is used.

Similar to (3.3) we have used in (3.5) $\tilde{\zeta} = \tilde{\zeta}_0 + \sum_{i \geq 1} \tilde{\zeta}_i$, with $\tilde{\zeta}_i = \text{Re}(\tilde{Z}_i e^{i(\mathbf{k}_i \cdot \mathbf{x} - \omega_i t)})$ for $i \geq 1$ and $\tilde{\zeta}_0 = \zeta_0$. Because of the strong coupling with the ζ_i , also the amplitudes \tilde{Z}_i of the $\tilde{\zeta}_i$ are smooth in space and slowly varying in time. So, using the same approximations as before (i.e., (3.4)) we obtain from (3.5):

$$\frac{\partial \zeta}{\partial t} = \sum_{i \geq 0} \frac{g \tilde{H}}{c_{\text{Bous},i}^2} \frac{\partial \tilde{\zeta}_i}{\partial t}, \quad \nabla \zeta = \sum_{i \geq 0} \frac{g \tilde{H}}{c_{\text{Bous},i}^2} \nabla \tilde{\zeta}_i, \quad (3.6)$$

where derivatives of \tilde{H} and the $c_{\text{Bous},i}$ have been neglected because the \tilde{Z}_i are small with respect to H and \tilde{H} , and because we assume that terms proportional to ∇h are negligible at boundaries.

Inserting the expressions (3.6) in (3.1), a separate system of equations for the convection component and each wave component i is obtained:

$$\frac{g \tilde{H}}{c_{\text{Bous},i}^2} \frac{\partial \tilde{\zeta}_i}{\partial t} + \nabla \cdot \mathbf{q}_i = 0, \quad (3.7)$$

$$\frac{\partial \mathbf{q}_i}{\partial t} + (\bar{\mathbf{u}} \cdot \nabla) \mathbf{q}_i + \bar{\mathbf{u}} (\nabla \cdot \mathbf{q}_i) - (\bar{\mathbf{u}} \bar{\mathbf{u}}^T) \frac{g \tilde{H}}{c_{\text{Bous},i}^2} \nabla \tilde{\zeta}_i + g \tilde{H} \nabla \tilde{\zeta}_i = \mathbf{P}'_{b,i} \nabla h. \quad (3.8)$$

The \mathbf{q}_i in these equations satisfy $\mathbf{q} = \mathbf{q}_0 + \sum_{i \geq 1} \mathbf{q}_i = \mathbf{q}_0 + \sum_{i \geq 1} \mathbf{Q}_i e^{i(\mathbf{k}_i \cdot \mathbf{x} - \omega_i t)}$, with smooth and slowly varying amplitudes $\mathbf{Q}_i(\mathbf{x}, t)$. This decomposition follows automatically.

The right-hand side of the momentum equations (3.8) satisfy $\sum_{i \geq 0} \mathbf{P}'_{b,i} = \mathbf{P}'_b$. The precise form of the $\mathbf{P}'_{b,i}$ is irrelevant, as these right-hand sides will be neglected later anyway assuming small ∇h near the boundaries. Remark that the definition of the $\mathbf{P}'_{b,i}$ could be extended to include the terms proportional to ∇h that have been neglected in (3.5) and (3.6). This too is irrelevant in the present analysis.

Notice that the systems of equations (3.7)–(3.8) are *not* uncoupled from each other. Some weak coupling is provided by the right-hand sides of the momentum equation, but there is also a (non-linear) coupling due to the depth-averaged velocity because of:

$$\bar{\mathbf{u}} = \frac{\mathbf{q}}{H} = \frac{\mathbf{q}_0 + \sum_{i \geq 1} \mathbf{q}_i}{h + \zeta_0 + \sum_{i \geq 1} \zeta_i}.$$

Furthermore, there is a (non-linear) coupling hidden in the wave celerities $c_{\text{Bous},i}$ that not only depend on the amplitude k_i of the wave numbers but also on total water depth H and auxiliary variable \tilde{H} (cf. (3.5)).

It is a trivial matter to write each system (3.7)–(3.8) in characteristic form. The characteristic equations are the combinations:

$$-\frac{\mathbf{k}_i^\perp \cdot \bar{\mathbf{u}}}{k_i} [\text{eq.(3.7)}] + \frac{\mathbf{k}_i^\perp}{k_i} \cdot [\text{eq.(3.8)}], \quad (3.9)$$

$$\left(c_{\text{Bous},i} \pm \frac{\mathbf{k}_i \cdot \bar{\mathbf{u}}}{k_i} \right) [\text{eq.(3.7)}] \mp \frac{\mathbf{k}_i}{k_i} \cdot [\text{eq.(3.8)}], \quad (3.10)$$

with the $\mathbf{k}_i^\perp = (-k_{s,i}, k_{n,i})^T$ vectors that have the same size as, but are orthogonal to, the wave number vectors \mathbf{k}_i , i.e., $|\mathbf{k}_i^\perp| = |\mathbf{k}_i| = k_i$ and $\mathbf{k}_i^\perp \cdot \mathbf{k}_i = 0$. The result of the evaluation of (3.9) reads:

$$\begin{aligned} & -\frac{\mathbf{k}_i^\perp \cdot \bar{\mathbf{u}}}{k_i} \left(\frac{g\tilde{H}}{c_{\text{Bous},i}^2} \frac{\partial \tilde{\zeta}_i}{\partial t} + \frac{g\tilde{H}}{c_{\text{Bous},i}^2} (\bar{\mathbf{u}} \cdot \nabla) \tilde{\zeta}_i \right) + \frac{\mathbf{k}_i^\perp}{k_i} \cdot \left(\frac{\partial \mathbf{q}_i}{\partial t} + (\bar{\mathbf{u}} \cdot \nabla) \mathbf{q}_i \right) + \\ & + g\tilde{H} \frac{\mathbf{k}_i^\perp}{k_i} \cdot \nabla \tilde{\zeta}_i = \frac{\mathbf{k}_i^\perp}{k_i} \cdot (\mathbf{P}'_{b,i} \nabla h), \end{aligned} \quad (3.11)$$

while the evaluation of (3.10) boils down to:

$$\begin{aligned} & \left(c_{\text{Bous},i} \pm \frac{\mathbf{k}_i \cdot \bar{\mathbf{u}}}{k_i} \right) \left(\frac{g\tilde{H}}{c_{\text{Bous},i}^2} \frac{\partial \tilde{\zeta}_i}{\partial t} + \frac{g\tilde{H}}{c_{\text{Bous},i}^2} \left(\left(\bar{\mathbf{u}} \mp c_{\text{Bous},i} \frac{\mathbf{k}_i}{k_i} \right) \cdot \nabla \right) \tilde{\zeta}_i \right) + \\ & \mp \frac{\mathbf{k}_i}{k_i} \cdot \left(\frac{\partial \mathbf{q}_i}{\partial t} + \left(\left(\bar{\mathbf{u}} \mp c_{\text{Bous},i} \frac{\mathbf{k}_i}{k_i} \right) \cdot \nabla \right) \mathbf{q}_i \right) + \\ & - \frac{c_{\text{Bous},i}}{k_i^2} \left[\mathbf{k}_i^\perp \cdot \bar{\mathbf{u}} \frac{g\tilde{H}}{c_{\text{Bous},i}^2} \mathbf{k}_i^\perp \cdot \nabla \tilde{\zeta}_i - \mathbf{k}_i^\perp \cdot ((\mathbf{k}_i^\perp \cdot \nabla) \mathbf{q}_i) \right] = \mp \frac{\mathbf{k}_i}{k_i} \cdot (\mathbf{P}'_{b,i} \nabla h). \end{aligned} \quad (3.12)$$

Because of (3.3) and conditions (3.4), the gradient of each ζ_i is essentially in the direction of the corresponding wave number vector \mathbf{k}_i for $i = 1, 2, \dots$. No wave number vector is associated with convection component ζ_0 , but we may use \mathbf{k}_0 to indicate the direction in which the largest space-time variations of ζ_0 occur. We therefore define \mathbf{k}_0 as the vector that satisfies the equation $\partial \nabla \zeta_0 / \partial t = \mathbf{k}_0 \partial \zeta_0 / \partial t$. The time derivatives are required to exclude any stationary slope present in water level component ζ_0 due to, e.g., a non-zero time-averaged flow over a sloped bottom. Obviously we have $|\mathbf{k}_0| \ll k_{\min}$ since otherwise the definition of ζ_0 is in contradiction with (3.4).

Remark that, strictly speaking, \mathbf{k}_0 is *not* a wave number vector and is *not* to be confused with a wave number vector (although it does have the correct dimension). We use \mathbf{k}_0 merely for convenience, to extend the applicability of the equations (3.11) and (3.12) with convection component $i = 0$. For the same reason long-wave celerity $c_{\text{Bous},0}$ has been defined. Notice that for $\mathbf{k}_0 \rightarrow 0$, (3.12) reduces to $\partial \tilde{\zeta}_0 / \partial t + \bar{\mathbf{u}} \cdot \nabla \tilde{\zeta}_0 = 0$. Substituting this in (3.11) yields $\partial \mathbf{q}_0 / \partial t + \bar{\mathbf{u}} \cdot \nabla \mathbf{q}_0 + g\tilde{H} \nabla \tilde{\zeta}_0 = \mathbf{P}'_{b,0} \nabla h$ which includes stationary effects. Both equations show that we are indeed dealing here with a component that is convected.

We now have that for all $i = 0, 1, \dots$ the variation of the ζ_i normal to the vectors \mathbf{k}_i is much smaller than in any other direction. The same applies to the $\tilde{\zeta}_i$ and the \mathbf{q}_i because of their smoothly and slowly varying amplitudes \tilde{Z}_i and \mathbf{Q}_i which has followed automatically from the way the decomposition of the solution has been constructed. As a result, all $|\mathbf{k}_i^\perp \cdot \nabla \tilde{\zeta}_i|$ and $|(\mathbf{k}_i^\perp \cdot \nabla) \mathbf{q}_i|$ are virtually zero, and hence the last term in the left-hand sides of (3.11) and (3.12) can be neglected for all $i = 0, 1, \dots$. Combined with the assumption that ∇h is small near the boundaries, this means that the equations (3.11) and (3.12) describe approximately for each solution component the locally independent transport of three Riemann invariants:

$$\begin{aligned} & -\frac{\mathbf{k}_i^\perp \cdot \bar{\mathbf{u}}}{k_i} \frac{g\tilde{H}}{c_{\text{Bous},i}^2} \partial \tilde{\zeta}_i + \frac{\mathbf{k}_i^\perp}{k_i} \cdot \partial \mathbf{q}_i \approx 0 \text{ along the lines } \frac{d\mathbf{x}}{dt} = \bar{\mathbf{u}}, \\ & \left(c_{\text{Bous},i} + \frac{\mathbf{k}_i \cdot \bar{\mathbf{u}}}{k_i} \right) \frac{g\tilde{H}}{c_{\text{Bous},i}^2} \partial \tilde{\zeta}_i - \frac{\mathbf{k}_i}{k_i} \cdot \partial \mathbf{q}_i \approx 0 \text{ along the lines } \frac{d\mathbf{x}}{dt} = \bar{\mathbf{u}} - c_{\text{Bous},i} \frac{\mathbf{k}_i}{k_i}, \\ & \left(c_{\text{Bous},i} - \frac{\mathbf{k}_i \cdot \bar{\mathbf{u}}}{k_i} \right) \frac{g\tilde{H}}{c_{\text{Bous},i}^2} \partial \tilde{\zeta}_i + \frac{\mathbf{k}_i}{k_i} \cdot \partial \mathbf{q}_i \approx 0 \text{ along the lines } \frac{d\mathbf{x}}{dt} = \bar{\mathbf{u}} + c_{\text{Bous},i} \frac{\mathbf{k}_i}{k_i}. \end{aligned} \quad (3.13)$$

However, because the component $i = 0$ represents only convection, while for $i \geq 1$ we have no convection but only a wave propagating in the direction of \mathbf{k}_i , per component i no information is transported in two of the three directions. For $i = 0$ no information propagates along the characteristic lines $d\mathbf{x}/dt = \bar{\mathbf{u}} \pm c_{\text{Bous},0} \mathbf{k}_0/k_0$, and for each $i \geq 1$ non-zero information propagates only along the characteristic line $d\mathbf{x}/dt = \bar{\mathbf{u}} + c_{\text{Bous},i} \mathbf{k}_i/k_i$. Remark that this is merely a consequence of the way the solution has been decomposed, i.e., of (3.3) with conditions (3.4). The result is that in addition we have:

$$\begin{aligned} & -\frac{\mathbf{k}_i^\perp \cdot \bar{\mathbf{u}}}{k_i} \frac{g\tilde{H}}{c_{\text{Bous},i}^2} \partial \tilde{\zeta}_i + \frac{\mathbf{k}_i^\perp}{k_i} \cdot \partial \mathbf{q}_i \approx 0 \text{ locally for } i \geq 1, \\ & \left(c_{\text{Bous},i} + \frac{\mathbf{k}_i \cdot \bar{\mathbf{u}}}{k_i} \right) \frac{g\tilde{H}}{c_{\text{Bous},i}^2} \partial \tilde{\zeta}_i - \frac{\mathbf{k}_i}{k_i} \cdot \partial \mathbf{q}_i \approx 0 \text{ locally for } \forall i, \\ & \left(c_{\text{Bous},i} - \frac{\mathbf{k}_i \cdot \bar{\mathbf{u}}}{k_i} \right) \frac{g\tilde{H}}{c_{\text{Bous},i}^2} \partial \tilde{\zeta}_i + \frac{\mathbf{k}_i}{k_i} \cdot \partial \mathbf{q}_i \approx 0 \text{ locally for } i = 0. \end{aligned} \quad (3.14)$$

Only Froude numbers smaller than one are considered ($|\bar{\mathbf{u}}| < c_{\text{Bous},i}$, $i = 0, 1, \dots$). We will now make the rather crude assumption that at a boundary it is sufficient to consider only two wave components: one that travels in positive n -direction at a speed $\bar{\mathbf{u}} + c_{\text{Bous}}^+ \mathbf{k}^+/k^+$ (i.e., $\bar{u}_n + c_{\text{Bous}}^+ k_n^+/k^+ > 0$), and one that travels in negative n -direction at a speed $\bar{\mathbf{u}} + c_{\text{Bous}}^- \mathbf{k}^-/k^-$ (i.e., $\bar{u}_n + c_{\text{Bous}}^- k_n^-/k^- < 0$), see Figure 1. The variation in auxiliary variable $\partial \tilde{\zeta}$ and depth-integrated velocity $\partial \mathbf{q}$ can then be written as:

$$\partial \tilde{\zeta} = \partial \tilde{\zeta}_0 + \partial \tilde{\zeta}^- + \partial \tilde{\zeta}^+, \quad \partial \mathbf{q} = \partial \mathbf{q}_0 + \partial \mathbf{q}^- + \partial \mathbf{q}^+. \quad (3.15)$$

Furthermore, we will assume the convection component to be negligible:

$$\|\partial \tilde{\zeta}_0\| \ll \|\partial \tilde{\zeta}^-\|, \|\partial \tilde{\zeta}^+\|, \quad \|\partial \mathbf{q}_0\| \ll \|\partial \mathbf{q}^-\|, \|\partial \mathbf{q}^+\|. \quad (3.16)$$

The relevant equations from (3.14) are then:

$$\begin{aligned} (\sin \theta^- \bar{u}_n - \cos \theta^- \bar{u}_s) \frac{g \tilde{H}}{(c_{\text{Bous}}^-)^2} \partial \tilde{\zeta}^- - \sin \theta^- \partial q_n^- + \cos \theta^- \partial q_s^- &= 0, \\ (c_{\text{Bous}}^- + \cos \theta^- \bar{u}_n + \sin \theta^- \bar{u}_s) \frac{g \tilde{H}}{(c_{\text{Bous}}^-)^2} \partial \tilde{\zeta}^- - \cos \theta^- \partial q_n^- - \sin \theta^- \partial q_s^- &= 0, \end{aligned} \quad (3.17)$$

$$\begin{aligned} (\sin \theta^+ \bar{u}_n - \cos \theta^+ \bar{u}_s) \frac{g \tilde{H}}{(c_{\text{Bous}}^+)^2} \partial \tilde{\zeta}^+ - \sin \theta^+ \partial q_n^+ + \cos \theta^+ \partial q_s^+ &= 0, \\ (c_{\text{Bous}}^+ + \cos \theta^+ \bar{u}_n + \sin \theta^+ \bar{u}_s) \frac{g \tilde{H}}{(c_{\text{Bous}}^+)^2} \partial \tilde{\zeta}^+ - \cos \theta^+ \partial q_n^+ - \sin \theta^+ \partial q_s^+ &= 0, \end{aligned} \quad (3.18)$$

$$\text{with: } \cos \theta^- = \frac{k_n^-}{k^-}, \quad \sin \theta^- = \frac{k_s^-}{k^-}, \quad \cos \theta^+ = \frac{k_n^+}{k^+}, \quad \sin \theta^+ = \frac{k_s^+}{k^+}.$$

Assumption (3.16) is very reasonable. Information that is convected is related to the vorticity of the flow which should be small since the 2D Boussinesq-type model has been derived from the irrotational 3D free-surface potential flow model (Borsboom, 1998). Locally (3.16) may not hold, in particular in regions where a breaking wave model is active. Globally, and especially at the boundaries (where no strong rotational velocity field can be imposed since that would be a model violation), the assumption should be valid.

Assumption (3.15) on the other hand may not be justified at all. The equations (3.17) and (3.18) can be obtained from (3.14) only if the $c_{\text{Bous},i}$ and the \mathbf{k}_i of all outgoing, respectively all incoming wave components are roughly equal, i.e., if all outgoing, respectively all incoming waves travel at approximately the same angle and phase speed. This is clearly not always a reasonable assumption, and hence simplified decomposition (3.15) yields the most important limitation of the present approach.

The only way to overcome this limitation is by discerning more than one outgoing, respectively incoming wave component in the design of the boundary conditions. The technique that we present in the next sections to develop weakly reflecting and partially reflecting boundary conditions seems to allow such an extension. It leads however to considerably more complicated expressions, so in the present project we will just assume (3.15) and (3.16) which allows us to use (3.17) and (3.18). The shortcomings of this approach and its consequences will be clarified in the presentation and the discussion of the results.

The approach that we follow here resembles that of (Luchini and Tognaccini, 1996) and is similar to the one proposed in (Van Dongeren and Svendsen, 1997), but extends it to include both non-linear and dispersive effects. Luchini and Tognaccini show that their weakly reflecting boundary condition is a generalisation of the first- and second-order absorbing boundary conditions of Engquist and Majda (1977) and a considerable improvement. Van Dongeren and Svendsen (1997) show that their boundary condition causes significantly less reflection errors than a Sommerfeld radiation condition. In other words, we may expect that the boundary conditions developed in this project will lead to far less spurious reflections than the commonly used Sommerfeld boundary condition and its higher-order extensions (Engquist and Majda, 1977) for a wider range of applications.

On the other hand, it can be envisaged that the present approach will not be able to strongly reduce reflections in situations with many different incoming and outgoing wave components, each travelling at a different speed and angle. We point out that Luchini and Tognaccini (1996) as well as Van Dongeren and Svendsen (1997) have not dealt with this situation, since they have considered neither dispersive waves nor multiple wave directions occurring simultaneously.

To conclude we remark that the analysis of the Boussinesq-type equations presented in this section could equally well have been formulated in terms of $\partial\zeta$'s and $\partial\mathbf{q}$'s instead of in $\partial\tilde{\zeta}$'s and $\partial\mathbf{q}$'s, by replacing terms of the form $(g\tilde{H}/c_{\text{Bous}}^2)\partial\tilde{\zeta}$ by the equivalent form $\partial\zeta$ (cf. (3.6)). This would even have led to simpler expressions. It has been observed however during the computations that, although the $\partial\tilde{\zeta}$ and the $\partial\mathbf{q}$ are in phase, a small phase shift can exist near the boundaries between the $\partial\zeta$ and the $\partial\mathbf{q}$ of some wave component. Analysis has shown that this is due to dispersion errors introduced by the approximate boundary condition (2.5) of dispersion equation (2.4). Since the boundary procedure described in the next sections is very sensitive to phase errors, it has been decided to use $\partial\tilde{\zeta}$ instead of $\partial\zeta$ wherever appropriate.

3.2 Seaward boundary: weakly reflecting

Incident waves at a seaward boundary can be specified by imposing any suitable combination of $\partial\tilde{\zeta}^+$ and $\partial\mathbf{q}^+$. The restriction is of course that the incident wave is specified properly, i.e., the imposed $\partial\tilde{\zeta}^+$ and $\partial\mathbf{q}^+$ should not be such that all incoming wave information cancels (this would occur if the combination describes in fact an outgoing wave component). The issue may seem somewhat academic at first sight since in practice it is virtually impossible to obtain the expressions for $\partial\tilde{\zeta}^+$ and $\partial\mathbf{q}^+$. The analysis in the previous section is based on the fact that decomposition (3.15) exists, but it is not to be used explicitly. However, using the properties (3.17)–(3.18) of that decomposition in combination with (3.6) and assumption (3.16), it is very easy to express $\partial\zeta_{bc}$ and $\partial\mathbf{q}_{bc}$ (i.e., the variation of

the unknowns themselves at the boundary) in terms of a specified incident wave (e.g., given water elevation ζ_{giv}) such that *only* the incident wave is specified:

$$\begin{aligned}
 & (c_{\text{Bous}}^- + \cos\theta^- \bar{u}_n + \sin\theta^- \bar{u}_s) \frac{\partial \zeta_{bc}}{\partial t} - \cos\theta^- \frac{\partial q_{n,bc}}{\partial t} - \sin\theta^- \frac{\partial q_{s,bc}}{\partial t} = \\
 & = (c_{\text{Bous}}^- + \cos\theta^- \bar{u}_n + \sin\theta^- \bar{u}_s) \frac{\partial \zeta_{bc}^+}{\partial t} - \cos\theta^- \frac{\partial q_{n,bc}^+}{\partial t} - \sin\theta^- \frac{\partial q_{s,bc}^+}{\partial t} = \\
 & = [c_{\text{Bous}}^- - (\cos\theta^- \cos\theta^+ + \sin\theta^- \sin\theta^+) c_{\text{Bous}}^+] \frac{\partial \zeta_{bc}^+}{\partial t} = \\
 & = [c_{\text{Bous}}^- - (\cos\theta^- \cos\theta^+ + \sin\theta^- \sin\theta^+) c_{\text{Bous}}^+] \frac{\partial \zeta_{giv}}{\partial t},
 \end{aligned} \tag{3.19}$$

where we have also used $g\tilde{H}/(c_{\text{Bous}}^-)^2 \partial \tilde{\zeta}^- = \partial \zeta^-$, etc. (cf. (3.5)) and $\partial \mathbf{q} = (\partial q_n, \partial q_s)^T$.

Because of the approximations involved, it is likely that the use of (3.19) will slowly lead to a deviation between the value of ζ_{giv} and the actual water level at the boundary as modelled by the Boussinesq-type equations. To prevent this, some correction should be added, i.e., instead of (3.19) we should use:

$$\begin{aligned}
 & \exp(\omega_{impl}) \frac{\partial \zeta_{bc}}{\partial t} - \frac{1}{c_{\text{Bous}}^- + \bar{u}_p} \left(\cos\theta^- \frac{\partial q_{n,bc}}{\partial t} + \sin\theta^- \frac{\partial q_{s,bc}}{\partial t} \right) = \\
 & = \left(\exp(\omega_{impl}) - \frac{\cos\Delta\theta c_{\text{Bous}}^+ + \bar{u}_p}{c_{\text{Bous}}^- + \bar{u}_p} \right) \frac{\partial \zeta_{giv}}{\partial t} + \omega_{expl} \omega^+ (\zeta_{giv} - \zeta_{bc}),
 \end{aligned} \tag{3.20}$$

with ω_{impl} and ω_{expl} the non-dimensional correction coefficients, ω^+ the frequency of the incident wave, $\Delta\theta = \theta^- - \theta^+$ the angle between the two wave directions, and $\bar{u}_p = \cos\theta^- \bar{u}_n + \sin\theta^- \bar{u}_s$ the projection of velocity vector $\bar{\mathbf{u}}$ onto the direction of the outgoing wave. Notice that also the vector $\partial \mathbf{q}_{bc}/\partial t$ appears in the form of its projection onto the direction of the outgoing wave.

Boundary condition (3.20) becomes equal to (3.19) if we take the parameters ω_{impl} and ω_{expl} both equal to zero. By taking $\omega_{impl} > 0$, a possible deviation between ζ_{bc} and ζ_{giv} is reduced ‘implicitly’; in the limit of $\omega_{impl} \rightarrow \infty$, (3.20) simplifies to $\partial \zeta_{bc}/\partial t = \partial \zeta_{giv}/\partial t$ and hence to $\zeta_{bc} = \zeta_{giv}$ provided that initially ζ_{bc} is equal to ζ_{giv} as well. On the other hand, $\omega_{expl} > 0$ reduces a growing difference between ζ_{bc} and ζ_{giv} ‘explicitly’; when an explicit time-integration scheme is used, the last term in the right-hand side of (3.20) is implemented explicitly and may ultimately lead to an additional time-step stability restriction. Nevertheless, this correction term must be included since it is the only term in (3.20) that detects a difference between ζ_{bc} and ζ_{giv} directly. In view of the properties of both correc-

tion mechanisms, it seems advisable to use only small values for ω_{expl} (in order not to create numerical stability problems) and to use a fairly large value for ω_{impl} if there is a need to compensate for rather strong deviations.

Notice that the implicit and explicit correction mechanism correct for the (possibly growing) difference between ζ_{bc} and ζ_{giv} , instead of for the difference between ζ_{bc}^+ and ζ_{giv} . The latter is what is actually needed, but impossible to realise directly. The consequence is that both correction mechanisms introduce spurious partial reflection, so they should only be used as far as necessary.

Besides condition (3.20) two more equations are to be applied at the boundary, partly as a consequence of the numerical scheme that is used. The first one describes the behaviour of the outgoing wave solution near the boundary, for which in principle any combination of continuity equation and momentum equations can be used. It is however preferable to apply the combination that prescribes only the outgoing wave. This combination follows from (3.18), so at a boundary we discretise the equation:

$$\begin{aligned} & \left(c_{Bous}^+ + \cos\theta^+ \bar{u}_n + \sin\theta^+ \bar{u}_s \right) [\text{cont.eq.}] + \\ & - \cos\theta^+ [n - \text{mom.eq.}] - \sin\theta^+ [s - \text{mom.eq.}] . \end{aligned} \quad (3.21)$$

Remark that (3.21) is *not* the combination for the outgoing characteristic. That one is obtained if c_{Bous}^+ and θ^+ in (3.21) are replaced by c_{Bous}^- and θ^- . But then an equation would be applied that might affect the incoming wave, which situation we want to avoid.

For the remaining convective part of the solution we apply either an equation or a boundary condition. At an outflow boundary ($q_{n,bc} < 0$), we could use the combination of equations that describes the convection along streamlines, but (3.18) suggests to use:

$$\begin{aligned} & \left(\sin\theta^+ \bar{u}_n - \cos\theta^+ \bar{u}_s \right) [\text{cont.eq.}] + \\ & - \sin\theta^+ [n - \text{mom.eq.}] + \cos\theta^+ [s - \text{mom.eq.}] , \end{aligned} \quad (3.22)$$

which is again a combination that does not say anything about the incoming wave.

If $q_{n,bc} \geq 0$, we must apply a second boundary condition:

$$\begin{aligned} & \left(\sin\theta^- \bar{u}_n - \cos\theta^- \bar{u}_s \right) \frac{\partial \zeta_{bc}}{\partial t} - \sin\theta^- \frac{\partial q_{n,bc}}{\partial t} + \cos\theta^- \frac{\partial q_{s,bc}}{\partial t} = \\ & = -\omega_{expl} \omega^+ \left(-\sin\theta^- q_{n,bc} + \cos\theta^- q_{s,bc} \right) . \end{aligned} \quad (3.23)$$

This expression imposes a zero velocity normal to the direction of the outgoing wave, to avoid spurious reflections that could otherwise appear in the form of convection. Actually, it imposes the variation in time of that velocity, which is similar to the procedures applied

before. This ensures at the same time that no abrupt changes at the boundary occur when the flow changes from outflow to inflow. The combination of time derivatives used in the left-hand side has been taken from (3.17); the right-hand side has been added to prevent or correct deviations from zero.

For the application of the boundary conditions and boundary equations (i.e., (3.20), (3.21), and (3.22) or (3.23)) the celerity and angle of both the incoming and the outgoing wave are required. The quality of the weakly reflecting boundary condition depends entirely on the accuracy with which c_{Bous}^+ , θ^+ , c_{Bous}^- and θ^- are determined. Finding good approximations of these variables is important for all boundary procedures developed in this project, so we will treat this subject separately in Section 3.4.

3.3 Landward boundary: partially reflecting or fully reflecting

A landward boundary is a closed boundary where we would like to impose a (zero) normal flow condition. A weakly reflecting boundary condition imposing the normal depth-integrated velocity $q_{n,giv}$ is similar to (3.20), is derived in the same way, and reads:

$$\begin{aligned} & \left(c_{\text{Bous}}^- + \bar{u}_p \right) \frac{\partial \zeta_{bc}}{\partial t} - \exp(\omega_{impl}) \cos \theta^- \frac{\partial q_{n,bc}}{\partial t} - \sin \theta^- \frac{\partial q_{s,bc}}{\partial t} = \\ & = \left(-\exp(\omega_{impl}) \cos \theta^- + \frac{c_{\text{Bous}}^- - \sin \theta^- \sin \theta^+ c_{\text{Bous}}^+ + \cos \theta^- \bar{u}_n}{\cos \theta^+ c_{\text{Bous}}^+ + \bar{u}_n} \right) \frac{\partial q_{n,giv}}{\partial t} + \quad (3.24) \\ & \quad - \omega_{expl} \omega^+ \cos \theta^- (q_{n,giv} - q_{n,bc}). \end{aligned}$$

Since at a closed boundary we would normally have $q_{n,giv} = 0$, this can be simplified to:

$$\begin{aligned} & \left(c_{\text{Bous}}^- + \bar{u}_p \right) \frac{\partial \zeta_{bc}}{\partial t} - \exp(\omega_{impl}) \cos \theta^- \frac{\partial q_{n,bc}}{\partial t} - \sin \theta^- \frac{\partial q_{s,bc}}{\partial t} = \\ & = \omega_{expl} \omega^+ \cos \theta^- q_{n,bc}. \quad (3.25) \end{aligned}$$

The signs in these two expressions may seem incorrect at first sight. However, keep in mind that angle θ^- pertains to the *outgoing* wave, i.e., $\cos \theta^- < 0$ (see Figure 1).

It is physically more correct to model a landward boundary by means of partial reflection, and to impose something like:

$$\begin{aligned}
& \left(c_{\text{Bous}}^- + \cos\theta^- \bar{u}_n + \sin\theta^- \bar{u}_s \right) \frac{\partial \zeta_{bc}^+}{\partial t} - \cos\theta^- \frac{\partial q_{n,bc}^+}{\partial t} - \sin\theta^- \frac{\partial q_{s,bc}^+}{\partial t} = \\
& = r \left[\left(c_{\text{Bous}}^- - \cos\theta^- \bar{u}_n + \sin\theta^- \bar{u}_s \right) \frac{\partial \zeta_{bc}^-}{\partial t} + \cos\theta^- \frac{\partial q_{n,bc}^-}{\partial t} - \sin\theta^- \frac{\partial q_{s,bc}^-}{\partial t} \right] + \quad (3.26) \\
& + \frac{c_{\text{Bous}}^- - \cos\Delta\theta c_{\text{Bous}}^+}{\cos\theta^+ c_{\text{Bous}}^+ + \bar{u}_n} \frac{\partial q_{n,giv}}{\partial t},
\end{aligned}$$

with r the reflection coefficient that may be any function of the other variables. For example, it may depend on quantities like wave number, wave angle, water depth or structure slope. A convenient way to realise a wave-number dependent r is to consider it as a function of $\cos\theta^-/c_{\text{Bous}}^-$ which includes both the effect of wave dispersion and the effect of wave angle, in combination with wave amplitude ζ_{bc} to include non-linear effects. This will be generally sufficient for the modelling of the required physical processes.

In the left-hand side of (3.26) we have used c_{Bous}^- and $\pi - \theta^-$ instead of c_{Bous}^+ and θ^+ . The phase speed of the outgoing wave is c_{Bous}^- , so that must also be the phase speed of the incoming wave that is reflected back ($\rightarrow c_{\text{Bous}}^+ = c_{\text{Bous}}^-$ in the *left*-hand side), while the angles must satisfy $\theta^- + \theta^+ = \pi$ ($\rightarrow \theta^+ = \pi - \theta^-$ in the *left*-hand side). In fact, the left-hand side and the first term in the right-hand side of (3.26) have been obtained from (3.13) in combination with (3.17) and (3.18), and model the partial reflection of outgoing information travelling at a speed $\bar{u} + c_{\text{Bous}}^- k^- / k^-$ in the form of incoming characteristic information travelling at a speed $\bar{u} + c_{\text{Bous}}^- S k^- / k^-$, with S the matrix that mirrors vectors with respect to the s -axis.

The second term in the right-hand side of (3.26) is equal to the first term in the right-hand side of (3.24) with $\omega_{impl} = 0$, and would be present if in addition to partial reflection we would like to impose an incident wave in terms of the normal depth-integrated velocity. The term vanishes if we impose the trivial closed boundary condition $q_{n,giv} = 0$. The c_{Bous}^+ and θ^+ in that term are *not* equal to c_{Bous}^- and $\pi - \theta^-$, since they really pertain to the phase speed and angle of the imposed incident wave. In fact, we have here the situation that the incoming wave may consist of two parts: the incident wave and the reflected part of the outgoing wave, each having their own phase speed and angle.

This situation cannot be handled properly because we consider only a single incoming wave component (assumption (3.15)). For the moment this is irrelevant, since we will only deal with partial reflection at a closed boundary where we have no incident wave ($q_{n,giv}$ and hence $\partial q_{n,giv}/\partial t$ are zero). The value of c_{Bous}^+ and θ^+ pertaining to the incident wave are then arbitrary and may just as well be taken equal to c_{Bous}^- and $\pi - \theta^-$. Using the properties (3.17) and (3.18) of (3.15) in combination with (3.6) and assumption (3.16), (3.26) can then be written as the left-hand side of:

$$\begin{aligned}
 & \left(\frac{1-r}{1+r} c_{\text{Bous}}^- + \cos \theta^- \bar{u}_n + \frac{1-r}{1+r} \sin \theta^- \bar{u}_s \right) \frac{\partial \zeta_{bc}}{\partial t} + \\
 & - \cos \theta^- \frac{\partial q_{n,bc}}{\partial t} - \frac{1-r}{1+r} \sin \theta^- \frac{\partial q_{s,bc}}{\partial t} = \\
 & = \omega_{expl} \omega^- \cos \theta^- \frac{(1-r)(c_{\text{Bous}}^- - \bar{u}_n) + r \bar{u}_{n,typ}}{(1+r)(c_{\text{Bous}}^- - \bar{u}_n)} q_{n,bc} .
 \end{aligned} \tag{3.27}$$

The right-hand side of this partially reflecting boundary condition is an ‘explicit’ correction term similar to the one added in (3.25). An ‘implicit’ correction mechanism is not required; a comparison with (3.25) shows that an increase of reflection coefficient r has the same effect. Conversely, the comparison shows that an increase of implicit correction coefficient ω_{impl} in (3.25) leads to a higher (spurious) reflection; this applies also to (3.20).

The scaling of the ‘explicit’ correction term is such that its effect is almost turned off when $r \rightarrow 1$, whereby (3.27) reduces to $\partial q_{n,bc}/\partial t = 0$. So full reflection means $q_{n,bc} = \text{constant}$, but not necessarily $q_{n,bc} = 0$. This will be corrected for by parameter $\bar{u}_{n,typ}$ that should be slightly larger than zero, e.g., equal to (a small fraction of) a typical value of \bar{u}_n .

Concerning the additional two equations required at a landward boundary we follow the same procedure as for a seaward boundary which has been described in Section 3.2. So we use boundary equation (3.21) and, depending on the direction of the flow, either boundary equation (3.22) or boundary condition (3.23), where the value of c_{Bous}^+ and θ^+ pertaining to the (non-existing) incident wave are again taken equal to c_{Bous}^- and $\pi - \theta^-$.

The behaviour of partially reflecting boundary condition (3.27) is not always well defined. For $|\theta^-| \rightarrow \pi/2$ we have $\cos \theta^- \rightarrow 0$, which means that the condition degenerates for waves that are (nearly) parallel to the boundary when $r = 1$. It is interesting to notice that when $\cos \theta^- \rightarrow 0$ (and hence $\sin \theta^- \rightarrow \pm 1$), condition (3.23) ‘takes over’ by prescribing a zero normal velocity. Special measures are required to ensure that this condition, and not equation (3.22), will be applied in such situations. Nevertheless, an additional equation for the tangential velocity component is still required when $|\theta^-| \rightarrow \pi/2$, to replace the degenerated condition (3.27). This equation can be found by considering derivatives in space instead of in time, for which the expressions (3.17) can be used as well. As a full investigation of this problem lies outside the scope of the present project, we will just mention the result:

$$\begin{aligned}
 & \left(c_{\text{Bous}}^- + \frac{1-r}{1+r} \cos \theta^- \bar{u}_n + \sin \theta^- \bar{u}_s \right) \frac{\partial \zeta_{bc}}{\partial n} + \\
 & - \frac{1-r}{1+r} \cos \theta^- \frac{\partial q_{n,bc}}{\partial n} - \sin \theta^- \frac{\partial q_{s,bc}}{\partial n} = 0 .
 \end{aligned} \tag{3.28}$$

The right-hand side of this equation does not have an ‘explicit’ correction term, since we do not know anything about the value of the normal derivatives at the boundary.

Equation (3.28) degenerates when $r = 1$ and $\theta^- \rightarrow 0$ which is no problem since then condition (3.27) can be used. But for $|\theta^-| \rightarrow \pi/2$ it reduces to $\bar{u}_s \partial \zeta_{bc} / \partial n - \partial q_{s,bc} / \partial n = 0$, i.e., to a symmetry condition for the tangential velocity component. This is precisely the kind of condition that one would like to apply in the case of waves parallel to a boundary. The boundary condition to be used at a landward boundary is therefore a θ^- -dependent average of (3.27) and (3.28).

Further development of such a boundary condition is deferred to the sequel of the present project where also another problem related to parallel waves has to be addressed: standing waves parallel to a landward boundary, since then we have two waves that are however neither incoming nor outgoing. In the applications considered in this project we distinguish therefore the following two situations:

- applications with clear incoming and outgoing waves (θ^-, θ^+ not equal to $\pm\pi/2$ at all boundaries): apply the weakly reflecting boundary procedure at all boundaries,
- applications with ‘1D’ waves (θ^-, θ^+ equal to $\pm\pi/2$ at the two side walls): apply the weakly reflecting boundary procedure only at the boundaries where we have incident and outgoing waves (and where θ^-, θ^+ are equal to $\pi, 0$), and symmetry conditions at the two side walls.

3.4 The details

The application of weakly reflecting boundary condition (3.20), partially reflecting boundary condition (3.27) and the other components of the boundary procedure require knowledge about the incident wave and the outgoing wave. The easy part is the determination of the variables that depend on the known incident wave.

If the imposed wave signal consists of only one harmonic wave component, frequency ω^+ is known. Its wave number k^+ is the solution of the equation (cf. (3.5)):

$$\left(\frac{\omega^+}{k^+}\right)^2 = \left(c_{\text{Bous}}^+\right)^2 = g \tilde{H} \frac{1 + (\alpha - 1/3)(k^+ H)^2}{1 + \alpha(k^+ H)^2}, \quad (3.29)$$

from which we also obtain the celerity c_{Bous}^+ of the incident wave.

The tangential component k_s^+ of the wave number vector of the incident wave can be obtained straightforwardly from the behaviour of the imposed wave along the boundary. The angle of incidence is given by:

$$\theta^+ = \arcsin(k_s^+ / k^+). \quad (3.30)$$

Smooth variations of ω^+ , k^+ and θ^+ in time and along the boundary are allowed, provided that the conditions (3.4) are still satisfied. However, these conditions cannot be satisfied anymore when a wave spectrum is imposed, because we consider only one incoming wave component. In that case, a typical value of ω^+ and k_s^+ needs to be determined, for example by writing the wave imposed at the boundary *locally* as:

$$\zeta_{giv}(s, t) = \bar{\zeta}_{giv} + Z_{giv} \sin(k_s^+ s - \omega^+ t - \varphi), \quad (3.31)$$

assuming constant offset $\bar{\zeta}_{giv}$, constant amplitude Z_{giv} , constant phase shift φ , and constant ω^+ and k_s^+ . A typical local value of these unknowns can be determined by solving approximately a sufficiently large number of equations (3.31) using, e.g., a non-linear least-squares procedure, where the left-hand sides are obtained from, e.g., the specified time series and where the equations are evaluated at a number of points (s, t) in space and in time around a certain position and time level at the boundary. The procedure should lead to values of ω^+ and k_s^+ that are sufficiently smooth in space and in time; k^+ and θ^+ are again obtained from (3.29) and (3.30).

Further development and implementation of this procedure lies outside the scope of the present work. It is however obvious that the discrepancy between the single values ω^+ , k^+ and θ^+ on the one hand, and the specified incident wave on the other hand, depends entirely on the spectrum of the imposed wave. The broader the spectrum, the larger the ‘mismatch’, and hence the larger the spurious reflections will be that result from the use of the developed boundary procedure. This error will probably be amplified by the fairly large values of ω_{impl} and ω_{expl} that may be required to compensate for the deviations caused by the reflections. Ultimately, it may turn out to be necessary to consider more than one incoming wave component; this is the only way to obtain a better match for an incident wave having a broad spectrum, since then several ω^+ , k^+ and θ^+ are available to provide that match.

Information about the outgoing wave has to be obtained from the difference between the wave solution in the neighbourhood of the boundary as computed by the Boussinesq-type model and the specified incident wave. The description of the behaviour of the incident wave near the boundary follows from the extension of (3.31) in normal direction, which we combine with (3.5) to get an expression in terms of $\tilde{\zeta}^+$. The result is, written in differential form:

$$\partial \tilde{\zeta}^+(\mathbf{x}, t) = \frac{(c_{Bous}^+)^2}{g\tilde{H}} \partial \zeta_{giv}(\mathbf{x}, t) = \frac{(c_{Bous}^+)^2}{g\tilde{H}} Z_{giv} \partial \sin(\mathbf{k}^+ \cdot \mathbf{x} - \omega^+ t - \varphi), \quad (3.32)$$

with $\mathbf{k}^+ = (k_n^+, k_s^+)^T$, $k_n^+ = k_n \cos \theta^+$ and $\mathbf{x} = (n, s)^T$. Substitution in (3.18) yields:

$$\begin{aligned}\partial \mathbf{q}^+(\mathbf{x}, t) &= \left(\frac{\mathbf{k}^+}{k^+} c_{\text{Bous}}^+ + \bar{\mathbf{u}} \right) \frac{g \tilde{H}}{(c_{\text{Bous}}^+)^2} \partial \tilde{\zeta}^+(\mathbf{x}, t) = \\ &= \left(\frac{\mathbf{k}^+}{k^+} c_{\text{Bous}}^+ + \bar{\mathbf{u}} \right) Z_{giv} \partial \sin(\mathbf{k}^+ \cdot \mathbf{x} - \omega^+ t - \varphi),\end{aligned}\quad (3.33)$$

with $k^+ = |\mathbf{k}^+|$. Combined with (3.15) and assumption (3.16), we obtain from (3.32) and (3.33) the approximations pertaining to the outgoing wave:

$$\begin{aligned}\partial \tilde{\zeta}^-(\mathbf{x}, t) &= \partial \tilde{\zeta}(\mathbf{x}, t) - \frac{(c_{\text{Bous}}^+)^2}{g \tilde{H}} Z_{giv} \partial \sin(\mathbf{k}^+ \cdot \mathbf{x} - \omega^+ t - \varphi), \\ \partial \mathbf{q}^-(\mathbf{x}, t) &= \partial \mathbf{q}(\mathbf{x}, t) - \left(\frac{\mathbf{k}^+}{k^+} c_{\text{Bous}}^+ + \bar{\mathbf{u}} \right) Z_{giv} \partial \sin(\mathbf{k}^+ \cdot \mathbf{x} - \omega^+ t - \varphi).\end{aligned}\quad (3.34)$$

When these expressions are substituted in (3.17), the result is a system of two equations for the two unknowns c_{Bous}^- and ω^- . Both space and time derivatives of $\tilde{\zeta}^-$ and \mathbf{q}^- can be used to create these equations, but the use of space derivatives is recommended because they are easier to approximate numerically: the same discretisations as used for the flow equations can be employed. The discretisation of time derivatives on the other hand should be as consistent as possible with the applied Runge-Kutta scheme. It is not clear at present how this should be realised, but it will certainly require the storage of the solution at all four Runge-Kutta stages. Time discretisations can also use only previous information and will therefore always lag a little in time. Because of these disadvantages the use of time derivatives to extract information about the outgoing wave has been discarded.

Using (3.34) we can now evaluate the coefficients in the equations:

$$\begin{aligned}(\cos \theta^- c_{\text{Bous}}^- + \bar{u}_n) \frac{g \tilde{H}}{(c_{\text{Bous}}^-)^2} \left(\frac{\partial \tilde{\zeta}^-}{\partial n}, \frac{\partial \tilde{\zeta}^-}{\partial s} \right) - \left(\frac{\partial q_n^-}{\partial n}, \frac{\partial q_n^-}{\partial s} \right) &= 0, \\ (\sin \theta^- c_{\text{Bous}}^- + \bar{u}_s) \frac{g \tilde{H}}{(c_{\text{Bous}}^-)^2} \left(\frac{\partial \tilde{\zeta}^-}{\partial n}, \frac{\partial \tilde{\zeta}^-}{\partial s} \right) - \left(\frac{\partial q_s^-}{\partial n}, \frac{\partial q_s^-}{\partial s} \right) &= 0,\end{aligned}\quad (3.35)$$

that have been obtained from (3.17). Notice that derivatives in both normal and tangential direction can be used.

The unknowns in the equations (3.35) are the combinations $\cos \theta^- c_{\text{Bous}}^-$ and $\sin \theta^- c_{\text{Bous}}^-$ from which the value of θ^- and c_{Bous}^- can be obtained. These values may however be very ill-determined. In particular, it may be that the result is a wave angle θ^- pointing *inward* ($-\pi/2 < \theta^- < \pi/2$), which would indicate that the dominant wave contained in $\partial \tilde{\zeta}^- - \partial \tilde{\zeta}^+$ and $\partial \mathbf{q}^- - \partial \mathbf{q}^+$ is a wave moving in positive and not in negative n -direction. This may occur for example in a situation where virtually no outgoing wave is present. More importantly, it

may *also* occur when the incident wave and/or the outgoing wave have a broad spectrum, because of the violation of the (in certain applications very crude) assumption that it is sufficient to consider only one incoming and one outgoing wave component. The differences $\partial\tilde{\zeta}^- - \partial\tilde{\zeta}^+$ and $\partial\mathbf{q}^- - \partial\mathbf{q}^+$ consist then largely of approximation errors of the boundary procedure and contain very little (if any) information about the outgoing wave.

A number of measures has been taken to compensate for these errors. Although some of them may introduce a small amount of spurious reflection, they guarantee a robust and reliable boundary treatment:

- To reduce the sensitivity of (3.35) to small local irregularities such as discretisation errors, the equations are evaluated at a small number of grid points around each point at the boundary and solved locally by means of a least-squares method.
- In the least-squares method, large coefficients have a dominant effect on the residual to be minimised. This means that wiggles in $\tilde{\zeta}^-$ and \mathbf{q}^- would have a relatively large effect on the least-squares solution of (3.35) which is totally undesirable. To obtain the opposite we use the inverse of (3.35).
- The solution of (3.35) is very sensitive to errors if the outgoing wave is small, and becomes undefined when no outgoing wave is present at all. Therefore, correction terms have been added to ensure that c_{Bous}^- and θ^- approach the default values c_{typ} and θ_{typ} for $\partial\tilde{\zeta}^-, \partial\mathbf{q}^- \rightarrow 0$. This may cause relatively large reflections but only if the outgoing waves are small which is acceptable.
- The determination of a single c_{Bous}^- and θ^- breaks down if the $\tilde{\zeta}^-$ and \mathbf{q}^- as computed from (3.34) do not represent a single harmonic wave. This situation occurs when the incident and/or the outgoing wave contain several wave components of equal importance that are quite different. The best possible alternative is to find the value of c_{Bous}^- and θ^- that roughly correspond with the ‘average’ wave behaviour of $\tilde{\zeta}^-$ and \mathbf{q}^- . Underrelaxation has been used to filter out that average behaviour while at the same time allowing it to vary slowly.

As a result of these measures the equations (3.35) become, using derivatives in normal direction (equations with derivatives in tangential direction are similar):

$$\begin{aligned}
 & \frac{(\cos\theta^- c_{\text{Bous}}^-)^2 + (\sin\theta^- c_{\text{Bous}}^-)^2}{g\tilde{H}(\cos\theta^- c_{\text{Bous}}^- + \bar{u}_n)} \left(\left| \frac{\partial\tilde{\zeta}^-}{\partial n} \right| + \delta\tilde{Z}_{\text{giv}} k_{\text{giv}} \right)^{-1} = \\
 &= \left(- \left| \frac{\partial q_n^-}{\partial n} \right| + \delta\tilde{Z}_{\text{giv}} k_{\text{giv}} (\cos\theta_{\text{typ}} c_{\text{typ}} + \bar{u}_n) \frac{g\tilde{H}}{c_{\text{typ}}^2} \right)^{-1}, \\
 & \frac{(\cos\theta^- c_{\text{Bous}}^-)^2 + (\sin\theta^- c_{\text{Bous}}^-)^2}{g\tilde{H}(\sin\theta^- c_{\text{Bous}}^- + \bar{u}_s)} \left(\left| \frac{\partial\tilde{\zeta}^-}{\partial n} \right| + \delta\tilde{Z}_{\text{giv}} k_{\text{giv}} \right)^{-1} = \\
 &= \left(- \left| \frac{\partial q_s^-}{\partial n} \right| + \delta\tilde{Z}_{\text{giv}} k_{\text{giv}} (\sin\theta_{\text{typ}} c_{\text{typ}} + \bar{u}_s) \frac{g\tilde{H}}{c_{\text{typ}}^2} \right)^{-1},
 \end{aligned} \tag{3.36}$$

$$\text{with: } \tilde{Z}_{giv} = \frac{1 + (\alpha - 1/3)(k_{giv}\tilde{H})^2}{1 + \alpha(k_{giv}\tilde{H})^2} Z_{giv}, \quad (3.37)$$

and with Z_{giv} and k_{giv} respectively a typical amplitude and a typical wave number of the imposed incident wave that could be varied in time as well as along the boundary. Instead of using (3.37), it is also possible (and more convenient) to specify \tilde{Z}_{giv} in (3.36) directly, or to specify $\tilde{Z}_{giv} k_{giv}$ which represents a typical amplitude of the gradient $\nabla\tilde{\zeta}^+$ (i.e., steepness of the incident wave). Small coefficient $\delta > 0$, typical celerity c_{typ} and typical wave angle θ_{typ} ensure that $c_{Bous}^- \rightarrow c_{typ}$ and $\theta^- \rightarrow \theta_{typ}$ for $|\partial\zeta^-/\partial n|, |\partial q_n^-/\partial n|, |\partial q_s^-/\partial n| \rightarrow 0$. On the other hand, large (and probably unreliable) values of $|\partial\zeta^-/\partial n|$, $|\partial q_n^-/\partial n|$ and $|\partial q_s^-/\partial n|$ reduce the relative importance of equation (3.36) in the least-squares procedure.

The derivatives in (3.36) are determined by means of underrelaxation:

$$\left| \frac{\partial\tilde{\zeta}^-}{\partial n} \right|^{next} = \omega_r \left| \frac{\partial\tilde{\zeta}^-}{\partial n} \right|^n + (1 - \omega_r) \left| \frac{\partial\tilde{\zeta}^-}{\partial n} \right|^{prev}, \quad (3.38)$$

with $\omega_r > 0$ the underrelaxation coefficient. The superscripts *next*, *n*, and *prev* denote respectively the value used in (3.36), the value of the derivative as calculated from (3.34), and the previous value used in (3.36). The other derivatives are underrelaxed in the same way.

When a very small ω_r is used, the result of (3.38) follows very slowly the actual derivative and tends to become roughly equal to the average value of $|\partial\tilde{\zeta}^-/\partial n|$ taken over a few wave periods. This is precisely the mechanism required to handle non-harmonic waves when only one outgoing wave component is considered. Since underrelaxation (3.38) is applied per numerical time step Δt , one has to make sure that non-dimensional coefficient ω_r is taken proportional to $\omega_{typ}\Delta t$, with ω_{typ} a typical wave frequency.

The equations (3.36) are now fully specified, although one small complication remains: they are non-linear in the unknowns $\cos\theta^- c_{Bous}^-$ and $\sin\theta^- c_{Bous}^-$. But these unknowns must vary slowly in time (and hence change very little per time step), because of the assumptions (3.4) that underlie the whole method. The least-squares method is therefore used to solve the equations (3.36) in linearised form, which approximation is perfectly acceptable.

This concludes the description of the boundary treatment. We point out that one aspect has not been taken into account yet. We have assumed that the incoming wave $\tilde{\zeta}^+, \mathbf{q}^+$ is formed only by the incident wave (cf. the expressions (3.32) and (3.33)), but in general it will also contain a reflected wave. It is important to include the latter as well, in order to get the best

possible approximation of the outgoing wave $\partial\tilde{\zeta}^- = \partial\tilde{\zeta} - \partial\tilde{\zeta}^+, \partial\mathbf{q}^- = \partial\mathbf{q} - \partial\mathbf{q}^+$. This issue will have to be dealt with once the extension to partially reflecting boundary conditions will be fully developed and implemented. However, it may also play a role here. Spurious reflections are also reflections, so including them in $\tilde{\zeta}^+, \mathbf{q}^+$ may lead to better approximations of $\partial\tilde{\zeta}^-, \partial\mathbf{q}^-$ and hence to less spurious reflections. The realisation of this non-linear feedback loop requires a reliable estimation of the amount of spurious reflection which may be very hard to obtain. We have not attempted yet to develop this interesting but complicated idea.

4 Validation of boundary conditions

4.1 Performance of weakly reflecting wave boundaries

To investigate the absorption properties of the boundary condition a similar problem is considered as the one described in Van Dongeren and Svendsen (1997). The absorption properties of the boundary conditions developed in this study are tested for a unidirectional wave propagating into a domain of constant depth $h = 0.5\text{m}$ for various angles of incidence θ (i.e., the angle between the wave propagation direction and the x -axis), wave periods T and wave amplitudes a . In the following examples waves are generated at the boundaries $x = 0$ and $y = 0$ only, and absorbed at all four boundaries.

The reflection properties are considered for a square domain

$$\Omega_1 = [(x, y) : 0 \leq x \leq 2\lambda, 0 \leq y \leq 2\lambda] ,$$

with the wave length $\lambda = 2\pi / k$. To make sure that the reflections are caused by one absorbing boundary (at $x = 2\lambda$) only, solutions are computed in two domains. The first computation is carried out on a large, square domain

$$\Omega_3 = [(x, y) : 0 \leq x \leq 4\lambda, 0 \leq y \leq 4\lambda] .$$

The second computation covers a smaller, rectangular domain

$$\Omega_2 = [(x, y) : 0 \leq x \leq 2\lambda, 0 \leq y \leq 4\lambda] .$$

See Figure 2 for a definition sketch.

The non-generating boundaries in domain Ω_3 are placed so far away that they have no effect on the solution in the smaller domain Ω_1 during the simulation. Therefore, the computational results inside domain Ω_1 can be considered free of reflection errors. The same holds for the second computation for which the non-generating boundary at $y = 4\lambda$ will not influence the solution in the smaller domain Ω_1 . Hence, the difference between the two solutions can only be caused by the absorbing boundary condition at $x = 2\lambda$.

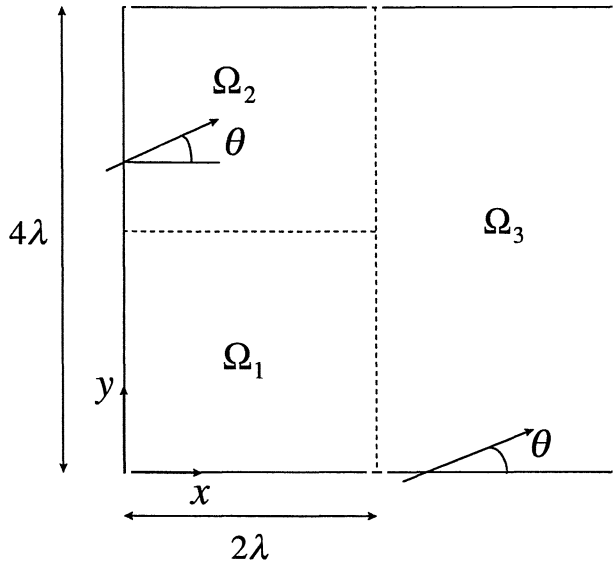


Figure 2: Definition sketch of domain used in reflection tests over horizontal bottom

At the boundaries $x = 0$ and $y = 0$ boundary equations (3.20) and (3.21) are imposed together with (3.22) or (3.23) depending on the direction of the normal component of the flow. At the other two boundaries (3.20) is replaced by (3.25). As already mentioned in Section 2.2 the boundary conditions (2.5) for the dispersion equation (2.4) are peculiar. In order to avoid strong wiggles in the auxiliary depth \tilde{H} and subsequently in the velocity components q , r and the total depth H in the upper left corner and lower right corner, these variables are obtained by constant extrapolation in the direction normal to the wave propagation direction at those corners.

All computations are carried out on an equidistant grid with $\Delta x = \Delta y = \lambda / 40$. The time step for the Runge Kutta time integrator is taken such that $CFL = \Delta t \sqrt{gh} / \Delta x = 2$. As mentioned in Chapter 3 several correction mechanisms are formulated to increase the robustness of the model. For the correction coefficients and relaxation parameters the following values have been used in all tests: $\omega_{impl} = 0$ and $\omega_r = 0.001$; $\omega_{expl} = 0.1$ at $x = 0$ and $y = 0$ and $\omega_{expl} = 0.01$ at the other boundaries. As much as possible incident wave information is used, hence $c_{typ} = c_{Bous}^+$, $\theta_{typ} = \theta^+$ and $\delta \tilde{Z}_{giv} k_{giv} = 0.1 k^+ a$. In order to avoid generation of short waves by starting abruptly at $t = 0$ a damping function is introduced, forcing the wave amplitude to increase smoothly in time towards the imposed wave amplitude a . The free surface elevation at $x = 0$ and $y = 0$ is specified as

$$\zeta_{giv}(\mathbf{x}, t) = a \sin(2\pi t/T - \mathbf{k}^+ \cdot \mathbf{x}) \left(\frac{1}{2} + \frac{1}{2} \tanh \left(\gamma_1 \frac{t - \gamma_2 T}{T} \right) \right), \quad (4.1)$$

for $\mathbf{x} = \mathbf{x}_{bc}$. For the tests in this section $\gamma_1 = 3.0$ and $\gamma_2 = 1.0$.

A measure for the reflection at the boundary $x = 2\lambda$ is defined as the normalised difference between the two solutions at the instant in time $t = t_n = \min(5T / \cos\theta, 5T / \sin\theta)$. At $t = t_n$ the initial condition has propagated out of Ω_1 ,

$$\varepsilon(x, y, t^n, \theta) = \frac{|\zeta_{\Omega_3}(x, y, t^n, \theta) - \zeta_{\Omega_2}(x, y, t^n, \theta)|}{a}, \quad (4.2)$$

where ζ_{Ω_3} and ζ_{Ω_2} are the solutions for the test runs in the domains Ω_3 and Ω_2 respectively. The average reflection error is quantified by introducing its spatial average over the grid points $\mathbf{x}_i = (x_i, y_i)$,

$$r(t^n, \theta) = \frac{1}{N} \sum_{i=1}^N \varepsilon(\mathbf{x}_i, t^n, \theta). \quad (4.3)$$

The definition of the reflection error (4.2) due to the absorbing boundary at $x = 2\lambda$ yields a spatial plot of this error. Three angles of incidence, $\theta = 0^\circ, 20^\circ, 45^\circ$, are considered in Figure F1a, F1b and F1c, where contour plots are given of the reflection errors for waves with $a=1.0$ cm, $T=1.5$ s. For $\theta = 0^\circ$ a 1D situation is obtained. As indicated at the end of Section 3.3 symmetry conditions are imposed at the ‘parallel’ boundaries $y = 0$ and $y = 4\lambda$. For the three situations the average reflection coefficients are listed in Table 1a. The angle information seems to be handled correctly. Nevertheless, Figure F1b and F1c show peculiar values of the reflection error near the lower-right corner. In Figure F2 the contour plot of the water level elevation is given for waves with $a=1.0$ cm, $T=1.5$ s and $\theta = 20^\circ$. Wiggles are observed in the lower-right region. These wiggles have a strong effect on the determination of the celerity and angle of the outgoing wave, resulting in spurious reflections. The reason for these wiggles to develop is due to the improper boundary conditions in the corner points, especially the one for \tilde{H} .

θ	r
0	0.028
20	0.041
45	0.064

Table 1a: Average reflection coefficients for $a=1.0$ cm, $T=1.5$ s

The effect of non-linear wave behaviour on the reflection properties is studied by considering different wave amplitudes. Figure F3 shows the average reflection error for the regime $T=1.5$ s, $\theta = 20^\circ$ and $a=5.0$ cm. The value of the reflection coefficient is $r = 0.046$ (see Table 1b), which is quite low. The result can be compared with Figure 1b where $a=1.0$ cm, so $\varepsilon = a/h = 0.02$ versus $\varepsilon = 0.1$. The average reflection coefficient obtained in the more non-linear situation is only slightly larger, $r = 0.046$ versus $r = 0.041$. This shows clearly that non-linear effects are fully taken into account in the boundary procedure.

a [cm]	$\varepsilon = ka$	r
1.0	0.02	0.041
5.0	0.1	0.046

Table 1b: Average reflection coefficients for $T=1.5$ s, $\theta = 20^\circ$

Finally the effect of linear dispersion on the reflection properties is studied by varying the wave period, and thus $\mu = kh$, for fixed angle of incidence $\theta = 20^\circ$ and wave amplitude $a=1.0$ cm. In Figure F4a, F4b the results are given for two wave regimes with $T = 1.0$ s and $T = 8.0$ s, corresponding with $\mu = 2.07$, and $\mu = 0.18$ respectively. The results can be compared with Figure 1b as well, where $T = 1.5$ s and thus $\mu = 1.11$. For the three situations the average reflection coefficients are given in Table 1c. The short waves apparently have more difficulties in predicting the correct incoming and outgoing wave components than the long waves. This behaviour is fully ascribed to the boundary conditions for the auxiliary depth \tilde{H} . For the long wave situation the reflection is small. This situation can be compared to Van Dongeren and Svendsen's (1997) results. They obtained average reflections of the order 0.02 for a similar problem. The present computational model seems to reflect less of the outgoing waves.

T [cm]	$\mu = kh$	r
1.0	2.07	0.055
1.5	1.11	0.041
8.0	0.18	0.009

Table 1c: Average reflection coefficients for $a=1.0$ cm, $\theta = 20^\circ$

4.2 Performance of model with 1D shoal

Beji and Battjes (1993) and Luth et al. (1994) have performed physical model tests of regular waves over an offshore bar in a wave flume. The geometric characteristics used in these two measurement campaigns are the same, except for the length scale, which in Luth et al. (1994) is twice as large as in Beji and Battjes (1993). Comparisons between several weakly non-linear Boussinesq-type models and experimental data by Beji and Battjes (1993) and Luth et al. (1994) have been presented by Dingemans (1994). For the sake of consistency with Dingemans' (1994) work, the data obtained by Luth et al. (1994) scaled to the scales of Beji and Battjes (1993) are applied in this test.

The bar consists of a 6.0 m long impermeable upward slope of 1:20, followed by a horizontal section of 2.0 m and a 3.0 m long downward slope of 1:10. The still water depth at the toe of the bar is 0.40 m, so the still-water depth at the top of the bar is 0.10 m. The experiments do have active wave absorption. Surface elevations are measured with wave gauges at several positions (see Table 2 for the exact location of the gauges). The layout of the experiment is given in Figure 3.

In the numerical experiment the incident waves at the left boundary ($x = 0$) are generated by imposing a sinusoidal wave, satisfying (4.1) with $\gamma_1 = 1.0$ and $\gamma_2 = 3.0$. The boundary procedure is identical to the 2D problem over a horizontal bed, which has been described in Section 4.1. The same correction coefficients have been applied.

Comparisons are shown between the measured and the computed surface elevation at 11 locations, which are given in Table 2. The time interval at which the results are plotted is chosen sufficiently long after the start so that permanent wave profiles are obtained in the farthest station.

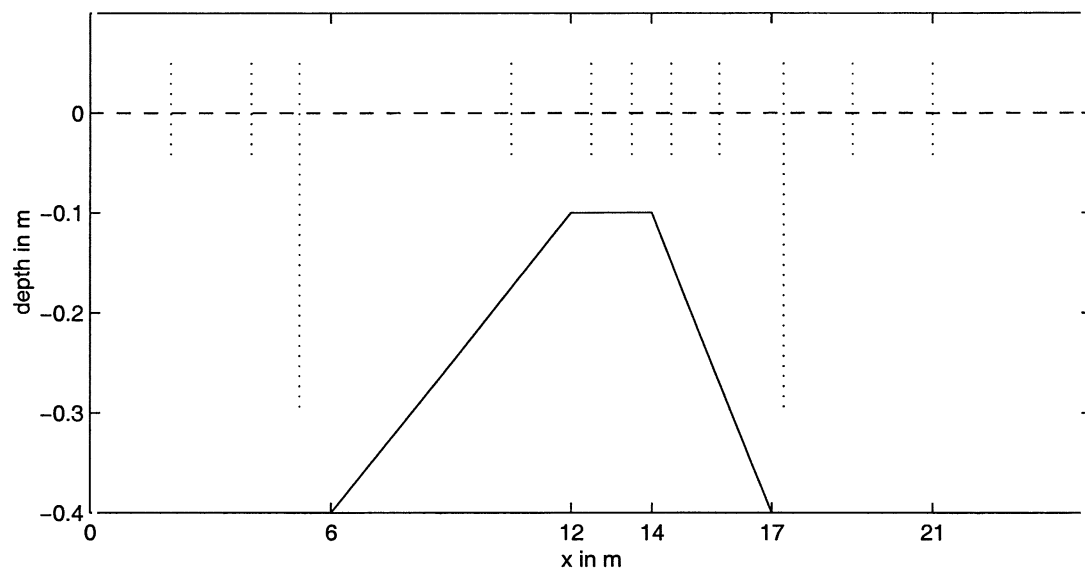


Figure 3: Bottom geometry and location of the wave gauges

Dingemans (1994) describes three measurement conditions. Here the non-breaking situation is considered, i.e. measurement condition A in Dingemans (1994). The imposed wave period and amplitude are $T = 2.02\text{s}$ and $a = 1.0\text{cm}$. The computations are carried out with $\Delta x = \Delta y = 0.05\text{m}$ and $\Delta t = 0.0505\text{s}$ for both conditions. Only 4 points are used in y -direction, since the symmetry conditions at the side walls yield a 1D situation.

Station	location (m)	remarks
1	2.0	close to wave maker
2	4.0	before the bar
3	5.2	just before the bar
4	10.5	on upward slope
5	12.5	on the bar
6	13.5	on the bar
7	14.5	on downward slope
8	15.7	on downward slope
9	17.3	just behind the bar
10	19.0	further behind the bar
11	21.0	far behind the bar

Table 2 Location of wave measuring stations.

In Figure F5 time series obtained from the computational model and the measurements are compared at the locations given in Table 1. The basic wave in this test is relatively long ($kh \approx 0.7$). Dingemans (1994) remarks that this test is such that on the first (upward) slope energy is transferred from the leading component to higher harmonics due to non-linear interactions, causing the wave to become steeper. The differences between the various Boussinesq-type models in this area and the horizontal area in front of the bar are negligible. Therefore, a good agreement between the measurements and the present Boussinesq-type model is not surprising. However, the second (downward) slope is

relatively steep and it is here where the differences between the various numerical models manifest themselves clearly. The model prediction of the wave form is good. On top of the bar a phase difference with the measured free surface elevation develops, which remains present down the slope and increases on the horizontal part behind the bar. Computations with smaller time step Δt and grid size $\Delta x, \Delta y$ showed that these phase differences disappear and that they are thus caused by numerical dispersion.

After $t \approx 20$ s the basic wave reaches the right boundary ($x=25$ m). To obtain a clear picture of the absorption properties the situation at $t_n = 50.5$ s is considered. In Figure 6 the reflection error (4.2) is plotted with $\Omega_3 = [x : 0 \leq x \leq 60\text{m}]$ and $\Omega_2 = [x : 0 \leq x \leq 25\text{m}]$. In the large flume the bar is at the same position as in the 25m long flume. The average reflection error equals $r = 0.053$. Figure F6 shows that this is a reduction of the error with a factor 2, compared to the situation where a long-wave assumption is made, i.e. $c_{\text{Bous}}^+ = c_{\text{Bous}}^- = \sqrt{gh} = 2.1\text{m/s}$. More precisely, $r = 0.083$. The latter approach coincides with the one proposed by Van Dongeren and Svendsen (1997).

In Figure F7 the computed outgoing wave celerity c_{Bous}^- at the two boundaries is given as a function of time. The presence of a broad spectrum of wave numbers requires a strong relaxation of the free surface and velocity gradients (cf. equation (3.38)). Here we used $\omega_r = 0.001$. Initially the wave celerity is set equal to the long-wave celerity. At both boundaries c_{Bous}^- converges to $c_{\text{typ}} = c_{\text{Bous}}^+$ almost instantly. Once the waves have reached the right boundary, the wave celerity predicted at the boundary decreases and fluctuates around a value in between the wave celerity corresponding to the basic frequency and the first higher harmonic. Time series analysis of the computed wave signal at a position at the end of the flume showed that these are the dominant frequency components. The dynamically determined wave celerity yields a better approximation than the larger initial wave celerity $c = c_{\text{Bous}}^+$ and even larger long wave celerity $c = \sqrt{gh}$. Also at the left boundary some modulation of the predicted outgoing wave celerity can be observed. However, the deviation from the typical wave celerity is small, because the steepness of the outgoing wave is relatively weak compared to a fraction of the typical wave steepness δka (equation (3.36)). The results show that the method is capable of determining a satisfying prediction of the outgoing wave (celerity) automatically.

4.3 Performance of model with 2D shoal

Finally the numerical model is applied to study monochromatic wave propagation over a two-dimensional shoal. The geometry used corresponds to the experimental arrangements of Berkhoff et al. (1982). The experimental geometry and locations of measurement transsects is shown schematically in Figure 4. Monochromatic waves with period $T = 1.0$ s and amplitude $a = 2.32\text{cm}$ are generated at $y = -10.0\text{m}$. The computational domain furthermore includes two vertical sidewalls, which are located at $x = -7.5\text{m}$ and $x = 7.5\text{m}$ and at which symmetry conditions are imposed. The boundaries at $y = 16.0\text{m}$ and $y = -10.0\text{m}$ are both absorbing boundaries. In order to reduce computational time, the original basin dimensions have been reduced. The wave heights along the indicated rays will be influenced hardly.

The bathymetry consists of an elliptic shoal resting on a plane slope of 1:50. Since only non-breaking waves are considered in this study, the original experimental set-up of Berkhoff et al. (1982) has been modified slightly. Where the (still-water) depth h becomes smaller than 10cm, the bed is considered horizontal. Bottom contours on the slope are oriented at an angle of -20° with respect to the x -axis. The bottom profile without shoal is given in meters by $h = 0.45$ for $y' < -5.82$; $h = \max(0.10, 0.45 - 0.02(5.82 + y'))$ for $y' \geq -5.82$. The boundary of the shoal is given by $(x'/4)^2 + (y'/3)^2 = 1$ and the thickness of the shoal is $d = -0.3 + 0.5\sqrt{1 - (x'/5)^2 - (y'/3.75)^2}$. The x' - y' co-ordinate system is obtained from the x - y system by rotating over -20° .

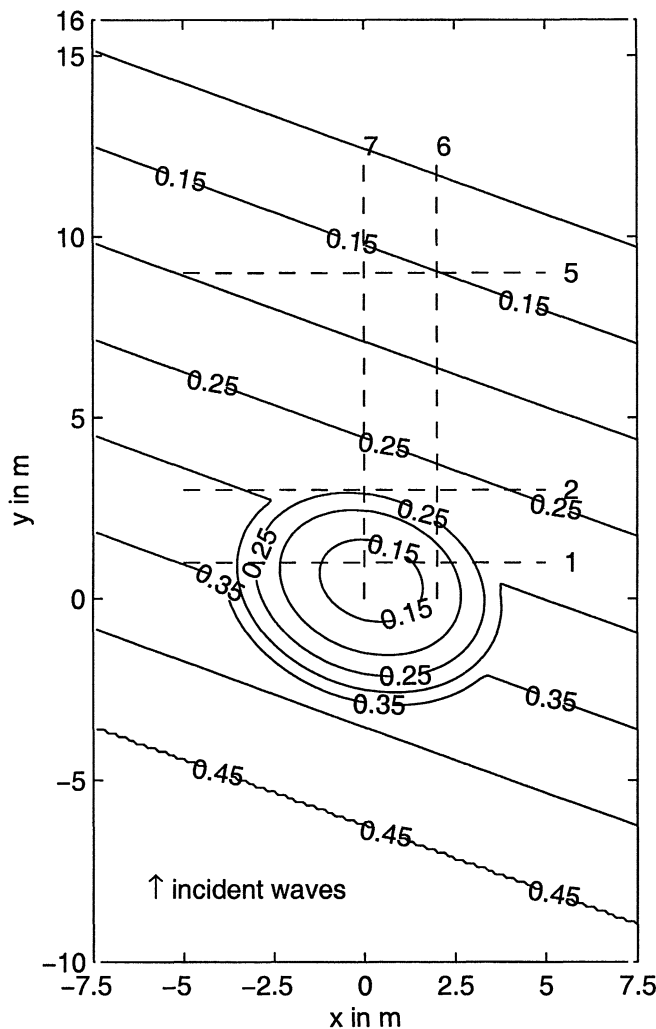


Figure 4: Bottom geometry of Berkhoff et al.'s (1982) 2D shoal

The computations have been carried out on a coarse grid, $\Delta x = \Delta y = 0.0625\text{m} \approx \lambda / 25$, using a timestep of $\Delta t = 0.05\text{s}$. Here λ denotes the wave length in the deeper part. Over the shoal shorter waves are generated. To ensure robustness we take $\omega_r = 0.001$. The other coefficients are the same as in the previous tests.

Wave heights along eight transects near the shoal were measured in the experiment. Periodic signal for the free surface elevation have been computed. The wave height is defined as the difference between maximum and minimum free surface elevation,

considered over a time interval in which the wave form is permanent. In Figure F8a and F8b the computed and measured wave heights are given, both relative to the incident wave height.

Obviously, the numerical results are not satisfying. As for the 1D bar in the previous section the wave height prediction is fairly good on the shoal. Once higher harmonics are propagating with their own celerity the wave height predictions become worse, see computational results for the transects 2, 5, 6 and 7. The reason for this disagreement needs further study. In the shallower parts of the basin the wave length will be shorter than in deeper water. In the shallower regions few grid points per wave length (approximately 8) are used compared to deep water. As a result the numerical accuracy is not satisfying in the shallower regions.

4.4 Discussion of results

A large number of aspects play a role when the reflection of dispersive waves at a boundary is considered:

- phase speed of incident and outgoing waves,
- angle of incident and outgoing waves,
- spectrum of incident and outgoing waves,
- non-linear effects,
- shoaling effects.

The first four items are taken into account in the developed boundary procedure. The local effect of shoaling is assumed to be negligible at boundaries.

The boundary procedure presented in this report is capable of handling both phase speed and wave angle. A separate incoming and outgoing wave has been considered whose phase speed and wave angle are respectively obtained from the specified incident wave or determined from the computed solution near the boundary. The procedure allows for variations of phase speed and wave angle in time as well as along the boundary. In the case of wave spectra the procedure attempts to determine a ‘best fit’, i.e., those phase speeds and wave angles that on average represent as good as possible the incoming and outgoing wave near the boundary. By considering the variations of water level and flow velocity in differential form, it was possible to retain the non-linear effects.

The procedure has been fully developed for weakly reflecting boundaries, but can be used also for totally reflecting boundaries that require rather trivial boundary conditions. It has been shown how the concept can be extended to partially reflecting boundaries, where some issues still need to be resolved. A procedure to handle waves that become parallel to the boundary needs to be developed (part of the solution has been given), and the effect of the reflected wave has to be taken into account in the determination of the incoming wave.

The approximation with the largest consequences is the rather crude assumption that it is sufficient to consider only one incoming and one outgoing wave. This is clearly not justified in situations with (broad) wave spectra. The test with the 1D shoal shows that in

spite of that good results can still be obtained: a reflection coefficient of only 5.3% was found for a rich outgoing wave signal (generated at the shoal) having several important higher harmonic components. Nevertheless we expect fairly large reflection errors in applications with broad wave spectra. For example, for a double-peaked wave spectrum the reflection could become as large as 20-30% because of the difference (mismatch) between the average phase speed c_{Bous}^- used in the boundary procedure and the phase speeds corresponding with the two dominant peaks. This is still considerably better than the usually applied long-wave Sommerfeld approximation which in these situations will lead to much higher reflections. In the 1D shoal test with its fairly narrow spectrum we found already that the long-wave Sommerfeld approximation introduces twice as much reflection than the developed boundary procedure. The only way to improve the performance of the method for broad wave spectra is by discerning more than just one incoming and one outgoing wave. The approach that we have followed allows for such an extension.

The 2D results obtained for wave propagation over a uniform bottom confirm that the method works well when a single wave component is considered. Reasonably low reflection coefficients were found for waves at different angles, phase speeds and amplitudes. The best results were obtained for long waves. This must be attributed to the local perturbation caused by the inadequate boundary condition of the dispersion equation. The effect of this error is of course most noticeable in short-wave simulations. This explains why in the calculations with the smaller wavelengths a larger reflection was observed.

One sensitive point of the method is that the outgoing wave is obtained by subtracting the incoming wave from the total solution. The estimation of the behaviour of the incoming wave near the boundary is analytical, which deviates in general slightly from how the incoming wave is computed by the numerical scheme. This leads to approximation errors in the estimation of the outgoing wave and hence to spurious reflections. A careful inspection of some of the results has confirmed this interpretation.

There may be an alternative way to reduce the sensitivity of the method: extract both the incoming and the outgoing wave from the numerical solution. This approach fits very well within the chosen framework but is a complicated extension of the already sophisticated boundary procedure. The advantage is that the effect of small errors near the boundary will then be included in the wave decomposition, so to some extent numerical imperfections will automatically be compensated for. It is a small step then to extend the method with a wave decomposition consisting of more than two wave components. An interesting aspect of this approach is that the least-squares ‘wave-fitting’ procedure will automatically detect the dominant wave components, independent of whether they are incoming or outgoing. Hence, if a better fit is possible by, e.g., using one incoming wave component and three outgoing wave components, then this will be taken care of automatically. The effect of partial reflection will be included as well. Notice however that the resulting algorithm will be substantially more complicated. In fact, we would then be attempting a local spectral analysis, using very few spectral components but optimising the wave frequency (phase speed) and wave angle to get the best possible spectral fit. This illustrates very well the basic idea behind the developed boundary procedure: use very few (presently two) components that are optimised automatically to get the best possible approximation of the waves at the boundary. The extension suggested here involves the use of more than two

components as well as a more elaborate technique to determine the incoming wave components, to obtain an even more accurate approximation.

5 Conclusions and recommendations

Based on the investigations described in this report the following conclusions and recommendations can be given:

Conclusions:

- A weakly reflecting boundary procedure for Boussinesq-type equations has been developed, and implemented successfully in an existing Boussinesq-type wave model. Reasonably low reflections of about 10 % (sometimes much lower) were obtained in a number of very different test cases. These results show that it is possible and very well feasible to design weakly reflecting boundary conditions by means of a sophisticated approach, using a local decomposition of the wave in incoming and outgoing wave components. The performance of the method is considerably better than the usually applied boundary conditions, especially in difficult applications with important non-linear effects and dispersion.
- The boundary procedure analyses the behaviour of the computed solution near the boundary and is therefore sensitive to small approximation errors in that solution. Several techniques have been designed and implemented to reduce the error sensitivity of the method. This has led to a considerable increase of the robustness of the method.
- We have shown how the approach can be used to develop a boundary condition that models the partial reflection at a landward boundary, where the reflection coefficient can be any function of variables such as wave angle, phase speed and wave amplitude. After resolving some remaining details the partially reflecting boundary condition is ready to be implemented.
- The incident waves used in the validation studies are all monochromatic. The extension to irregular incident waves by means of a procedure that extracts the dominant phase speed and wave angle from the given time series has been developed and is ready for implementation.
- The weakly reflecting boundary procedure makes the Boussinesq-type model very well suitable for integration in a nesting or domain decomposition framework, where it is important to avoid spurious reflections at the interfaces (internal boundaries) as much as possible.

Recommendations:

- It should be investigated whether it is necessary and possible to extract information about the incoming and outgoing wave components simultaneously from the computed solution. This takes care automatically of model imperfections and is therefore more accurate, and fits very well within the developed framework. Likewise, it should be investigated whether it is useful to consider more than one incoming and outgoing wave component. The analysis indicates that this will very likely be required if waves with broad spectra are to be handled properly.

- The boundary procedure developed for irregular incident waves needs to be implemented. Such an extension is required for practical applications as well as for the use of the Boussinesq-type model in a nesting or domain decomposition framework. The method that is proposed to obtain the dominant phase speed and wave angle from the time series specifying an irregular incident waves involves the use of a non-linear least-squares method and might be rather sensitive. This sensitivity is expected to be much smaller with the approach suggested in the previous recommendation.
- Irregular waves are generated by imposing a free surface elevation at the boundary that consists of a full spectrum of wave frequencies. By applying Fourier analysis the given energy density spectrum can be translated to a time series for the wave height. This also holds for the direction spreading. Time series for the angle of incidence can be determined by Fourier analysis, allowing the generation of both long-crested and short-crested waves. The boundary procedure developed in this project can be applied for both regimes. For short-crested waves it may be advantageous to consider several incoming and outgoing wave components (cf., the first recommendation). This will yield better predictions of the local wave celerities and wave angles.
- The remaining details of the partially reflecting boundary conditions need to be resolved, after which this extension is ready to be implemented. One detail concerns the contribution of the partially reflected wave to the incoming wave which effect has to be taken into account. If the first recommendation is developed, then this effect will be included automatically as well. In that case there is no need to design a technique for obtaining an estimation of the size of the reflected wave, which would eliminate a source of inaccuracies.
- With the developed boundary procedure, the coupling with a spectral wave model like SWAN must consist of an intermediate step where the results of the spectral wave model are translated to time series. Subsequently the dominant incoming wave component(s) is (are) to be extracted from those time series. If the number of wave components is kept variable, then it may be possible to couple SWAN and the Boussinesq-type model directly by transferring the spectral solution of SWAN to the incoming wave components of the Boussinesq-type model. This would eliminate quite a few sources of error since the incoming wave components would then not have to be determined anymore. It may be worth investigating this option more closely.
- The applications that have been considered are suitable for the validation of several aspects of the developed boundary procedure, but have all a monochromatic incident wave. To fully assess the performance of the method, also applications with irregular incident waves need to be considered.
- The remaining reflection error of the developed weakly reflecting boundary condition is due to the assumption that it is sufficient to consider only one incoming and one outgoing wave component (an approximation in situations with irregular waves), due to the boundary condition of the dispersion equation (introduces locally small short-wave errors), and due to numerical discretisation errors. A further improvement of the method should therefore concentrate on either one of these aspects.

References

- Beji, S. and J.A. Battjes (1993), *Experimental investigations of wave propagation over a bar*, Coastal Engrg. **19**, 151—162.
- Berkhoff, J.C.W., N. Booy and A.C. Radder (1982), *Verification of numerical wave propagation models for simple harmonic linear water waves*, Coastal Engrg. **6**, 255—279, Elsevier, Amsterdam.
- Berkhoff, J.C.W. (1982), *Refraction and diffraction of water waves. Wave deformation by a shoal. Comparison between computations and measurements*, Delft Hydraulics Report W 154 part VIII.
- Borsboom, M. (1998), *A Boussinesq-type wave model with improved linear and non-linear behaviour*, Delft Hydraulics Report H2303.51/X0231.40.
- Borsboom, M., N. Doorn, J. Groeneweg and M. Van Gent (2000), *A Boussinesq-type wave model designed for efficiency that conserves both mass and momentum*, paper accepted for presentation at the 27th Int. Conf. on Coastal Engineering, Sydney, Australia.
- Dingemans, M.W. (1994), *Comparison of computations with Boussinesq-like models and laboratory measurements*, Delft Hydraulics Report H1684.
- Dingemans, M.W. (1997), *Water Wave Propagation over Uneven Bottoms, Part 2—Non-linear Wave Propagation*, World Scientific, Singapore.
- Dingemans, M.W. and L.M. Merckelbach (1997), *Boussinesq-like equations with higher-order frequency dispersion*, Preprint, Delft Hydraulics.
- Engquist, B. and A. Majda (1977), *Absorbing boundary conditions for the numerical simulation of waves*, Math. Comput. **31**, 629—651.
- Gobbi, M.F. and J.T. Kirby (1999), *Wave evolution over submerged sills: tests of a high-order Boussinesq model*, Coastal Engrg. **37**, 57—96, Elsevier, Amsterdam.
- Luchini, P. and R. Tognaccini (1996), *Direction-adaptive nonreflecting boundary conditions*, J. Comput. Phys. **128**, 121—133.
- Luth, H.R., G. Klopman and N. Kitou (1994), *Project 13G: Kinematics of wave breaking partially on an offshore bar; LDV measurements for waves with and without a net offshore current*, Delft Hydraulics Report H1573.
- Madsen, P.A. and O.R. Sørensen (1992), *A new form of the Boussinesq equations with improved linear dispersion characteristics. Part 2. A slowly-varying bathymetry*, Coastal Engrg. **18**, 183—204, Elsevier, Amsterdam.
- Madsen, P.A. and H.A. Schäffer (1998), *Higher-order Boussinesq-type equations for surface gravity waves: derivation and analysis*, Phil Trans. R. Soc. Lond. A **356**, 3123—3184.
- Nwogu, O. (1993), *Alternative form of Boussinesq equations for nearshore wave propagation*, J. of Waterway, Port, Coastal and Ocean Engrg. **119**, 618—638, ASCE.
- Schäffer, H.A. and P.A. Madsen (1995), *Further enhancements of Boussinesq-type equations*, Coastal Engrg. **26**, 1—14.
- Van Dongeren, A.R. and I.A. Svendsen (1997), *Absorbing-generating boundary condition for shallow-water models*, J. of Waterway, Port, Coastal and Ocean Engrg. **123**, 301—313, ASCE.
- Wei, G., J.T. Kirby, S.T. Grilli and R. Subramanya (1995), *A fully non-linear Boussinesq model for surface waves. Part I. Highly non-linear unsteady waves*, J. Fluid Mech. **294**, 71—92.

Figures

Figures

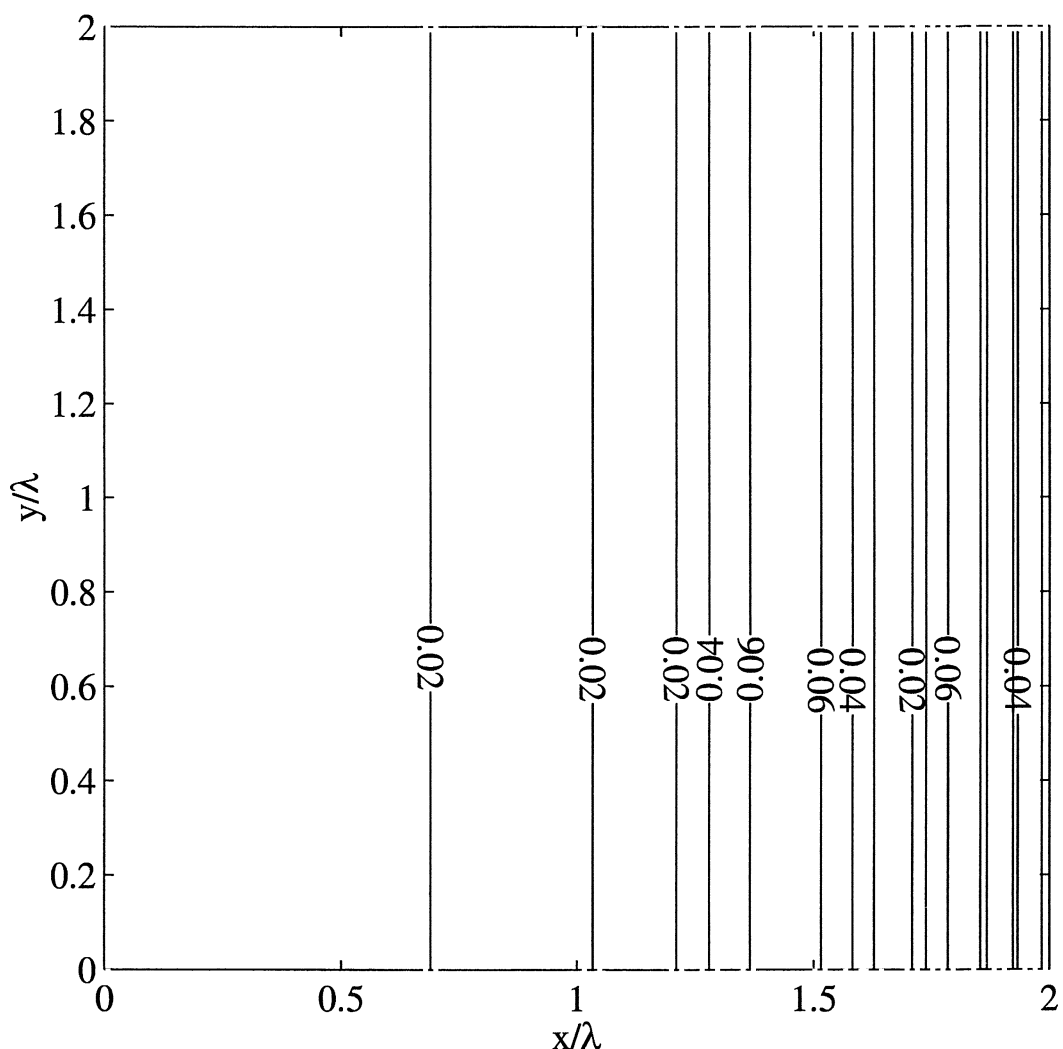


Figure F1a Reflection errors for wave amplitude $a = 1.0\text{cm}$, wave period $T = 1.5\text{s}$ and angle of incidence
 $\theta = 0^\circ$ at $t = 7.04\text{s}$

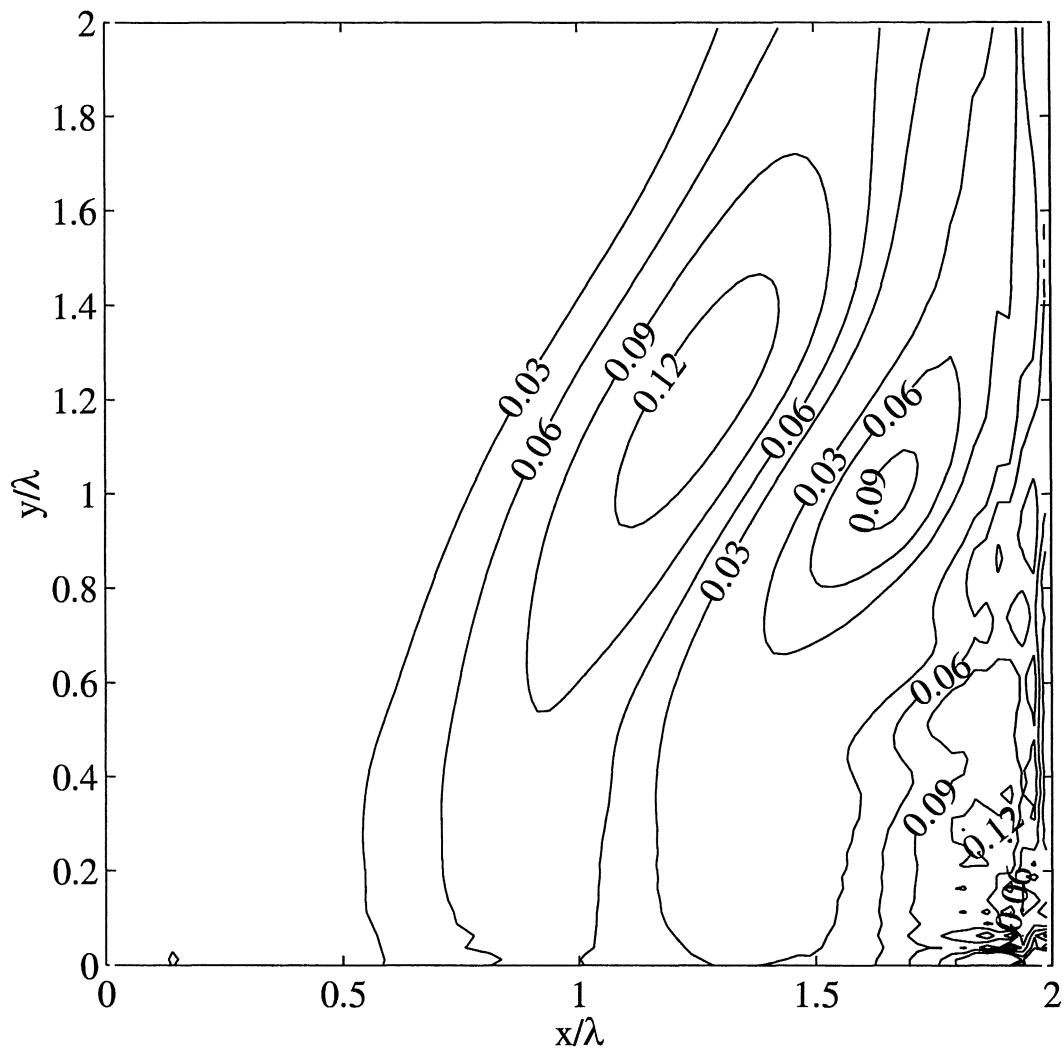


Figure F1b Reflection errors for wave amplitude $a = 1.0\text{cm}$, wave period $T = 1.5\text{s}$ and angle of incidence $\theta = 20^\circ$ at $t = 7.68\text{s}$

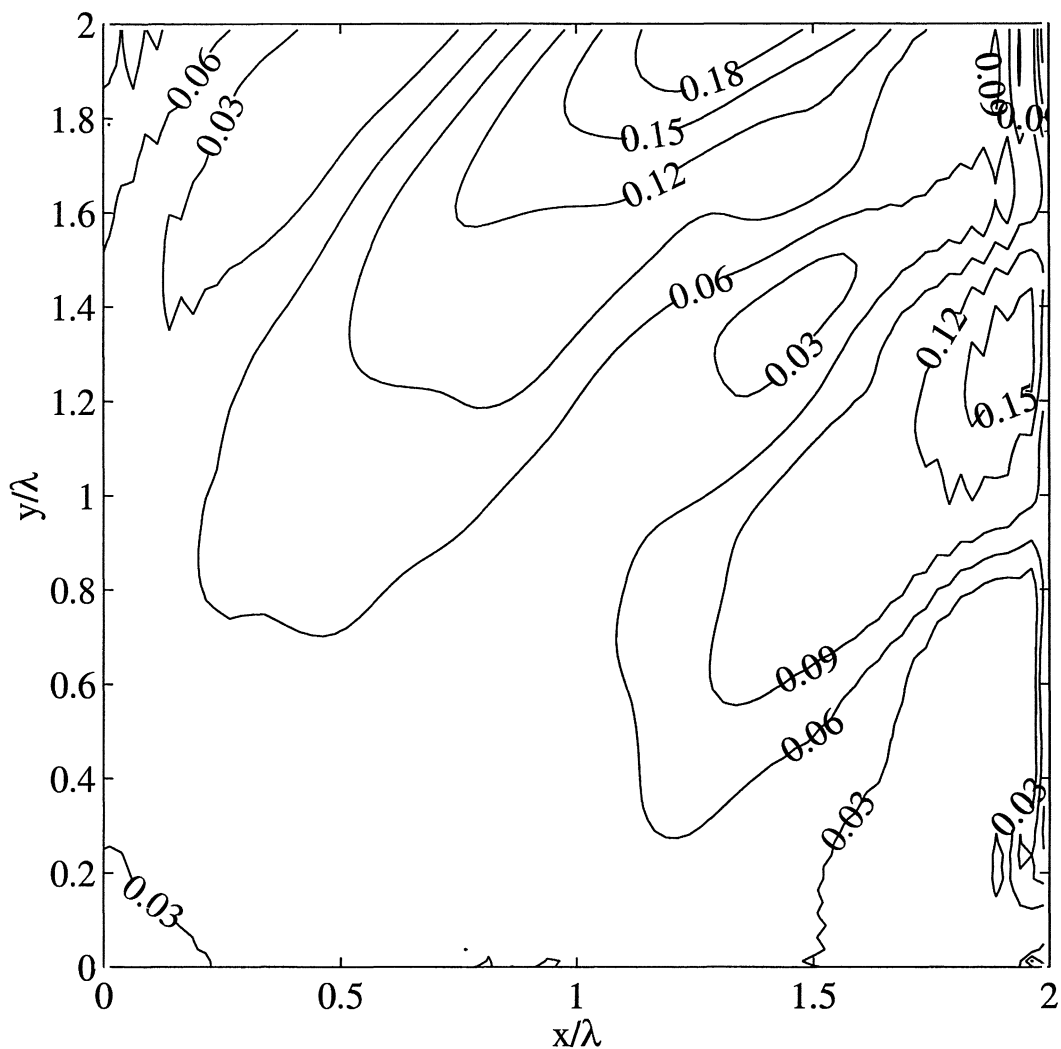


Figure F1c Reflection errors for wave amplitude $a = 1.0\text{cm}$, wave period $T = 1.5\text{s}$ and angle of incidence $\theta = 45^\circ$ at $t = 10.24\text{s}$

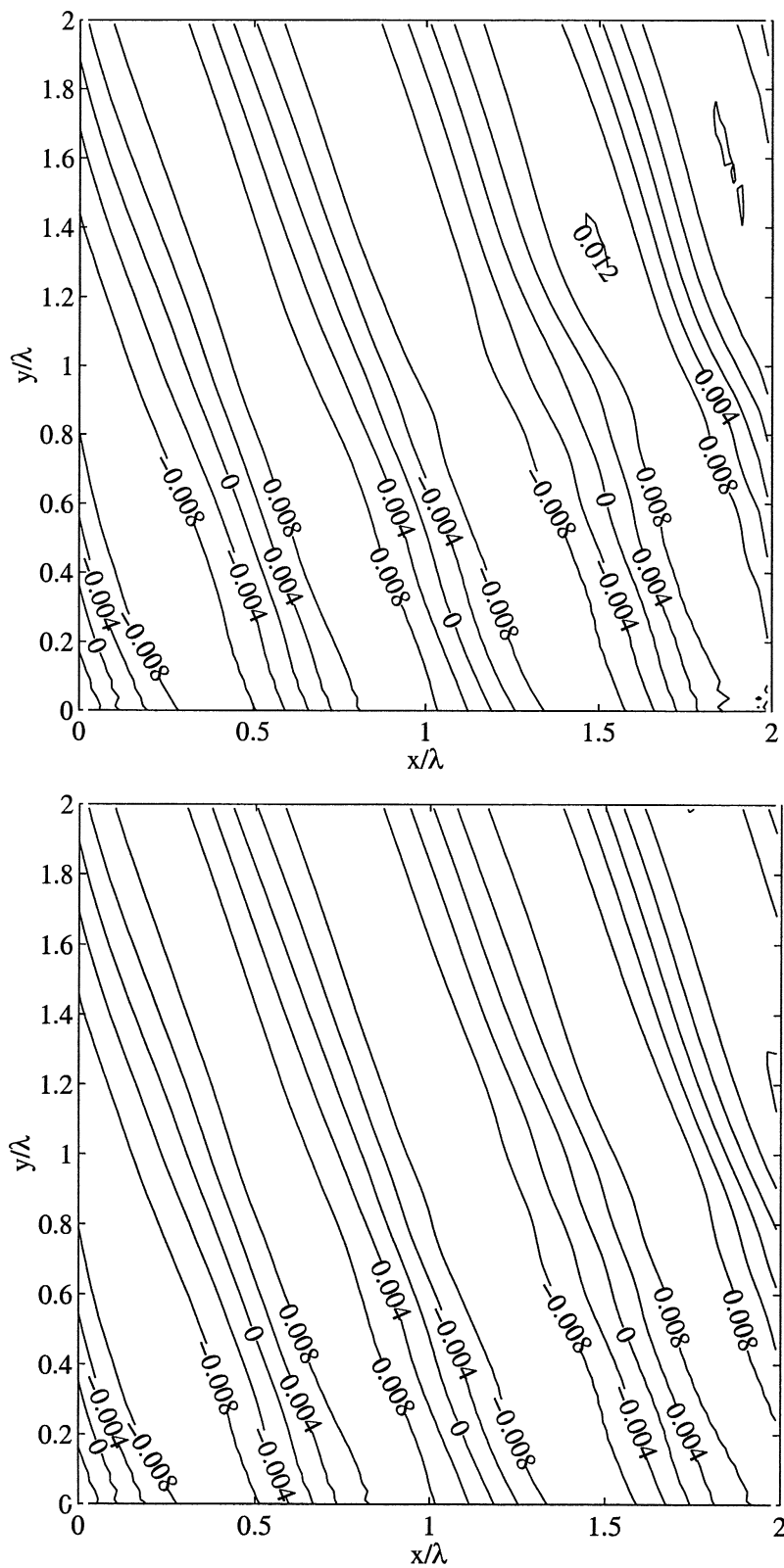


Figure F2: Water level elevation computed in Ω_2 (upper figure) and in Ω_3 (lower figure) for waves with
 $a = 1.0\text{cm}$, $T = 1.5\text{s}$ and $\theta = 20^\circ$

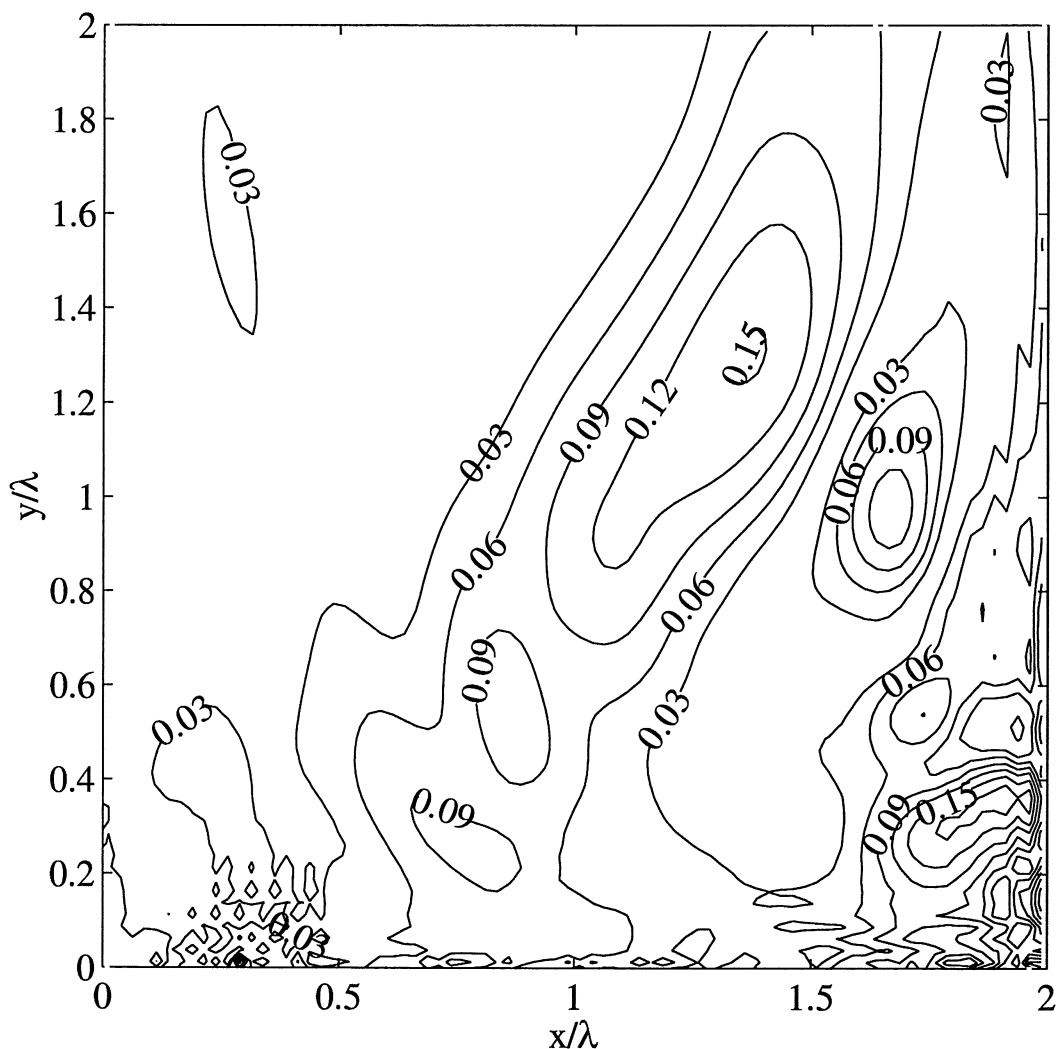


Figure F3: Reflection errors for wave amplitude $a = 5.0\text{cm}$, wave period $T = 1.5\text{s}$ and angle of incidence $\theta = 20^\circ$ at $t = 7.68\text{s}$

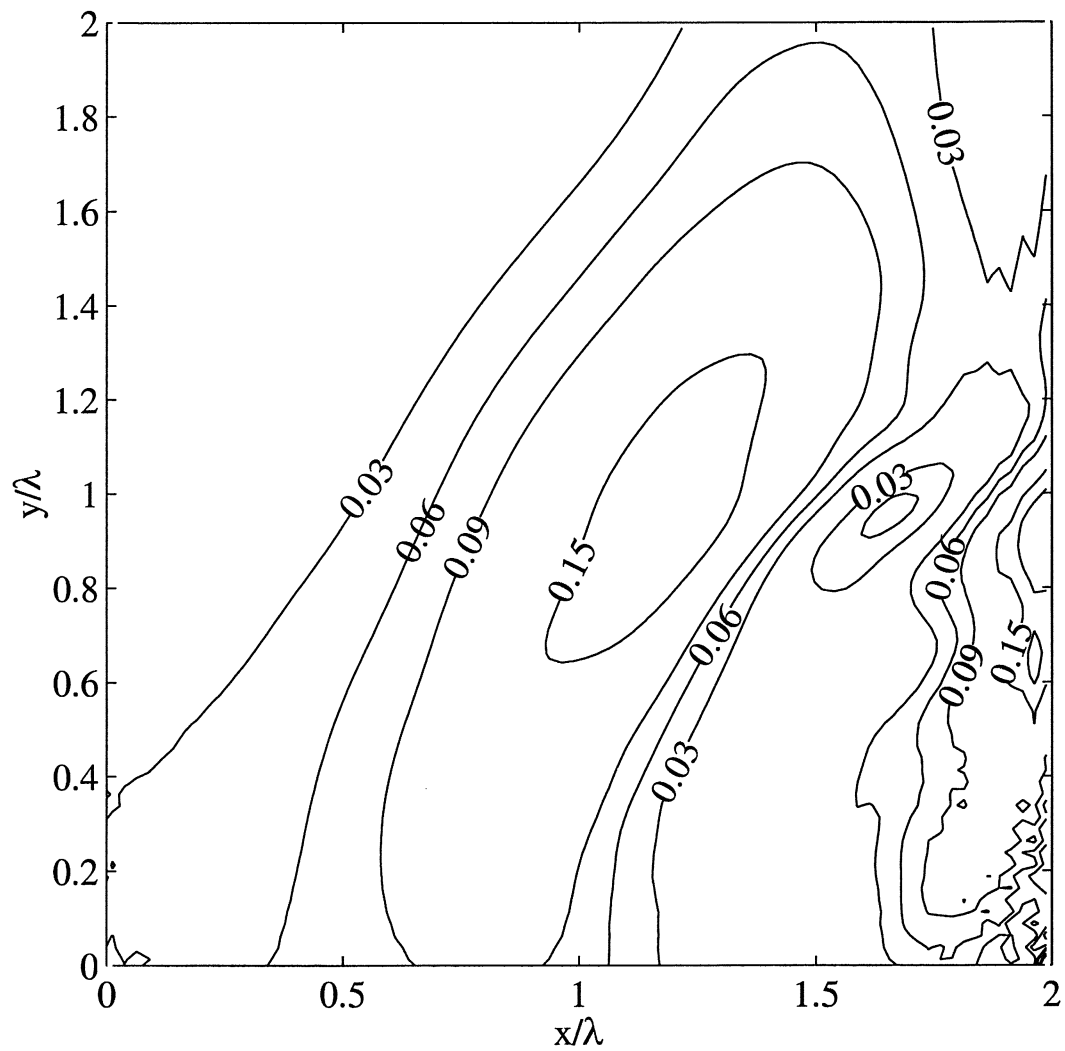


Figure F4a: Reflection errors for wave amplitude $a = 1.0\text{cm}$, wave period $T = 1.0\text{s}$ and angle of incidence $\theta = 20^\circ$ at $t = 5.1\text{s}$

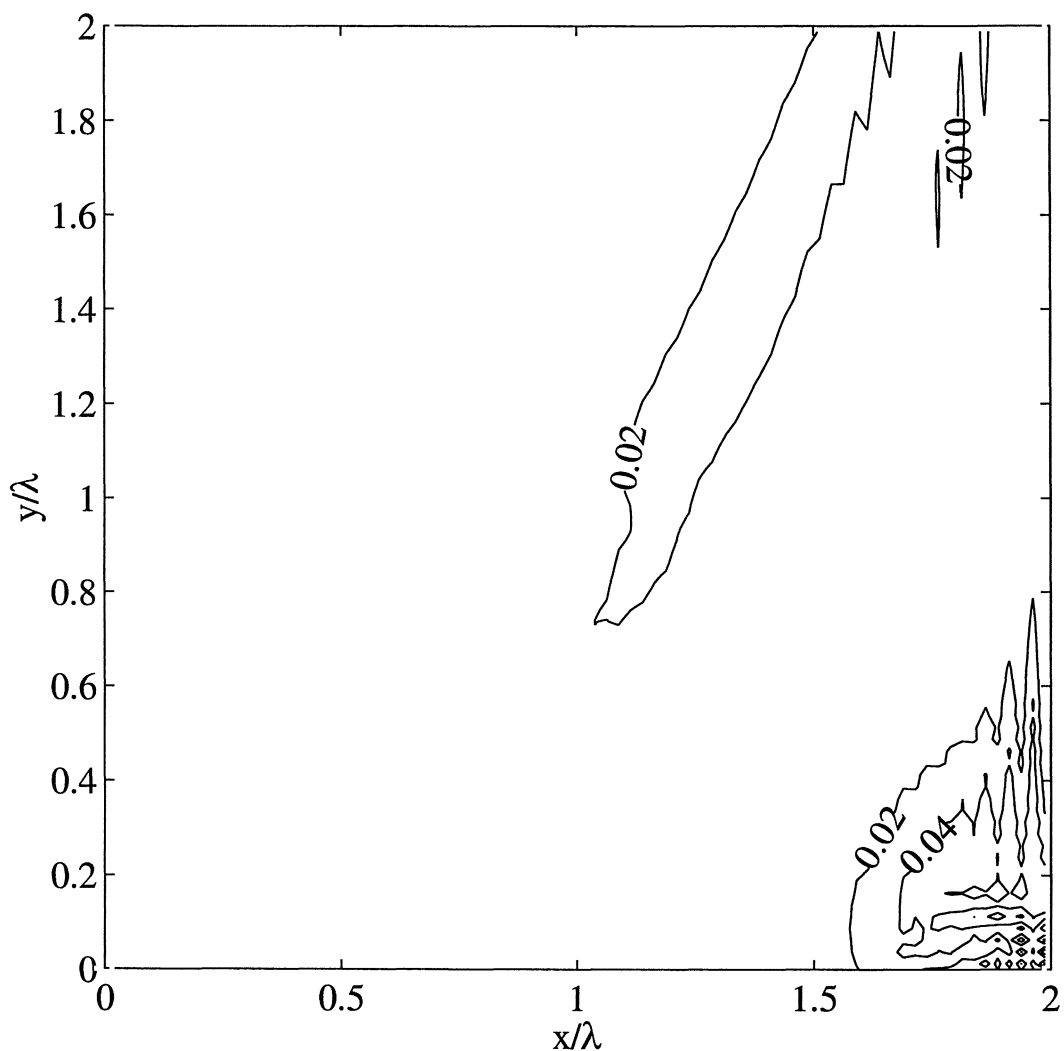


Figure F4b: Reflection errors for wave amplitude $a = 1.0\text{cm}$, wave period $T = 8.0\text{s}$ and angle of incidence $\theta = 20^\circ$ at $t = 40.0\text{s}$

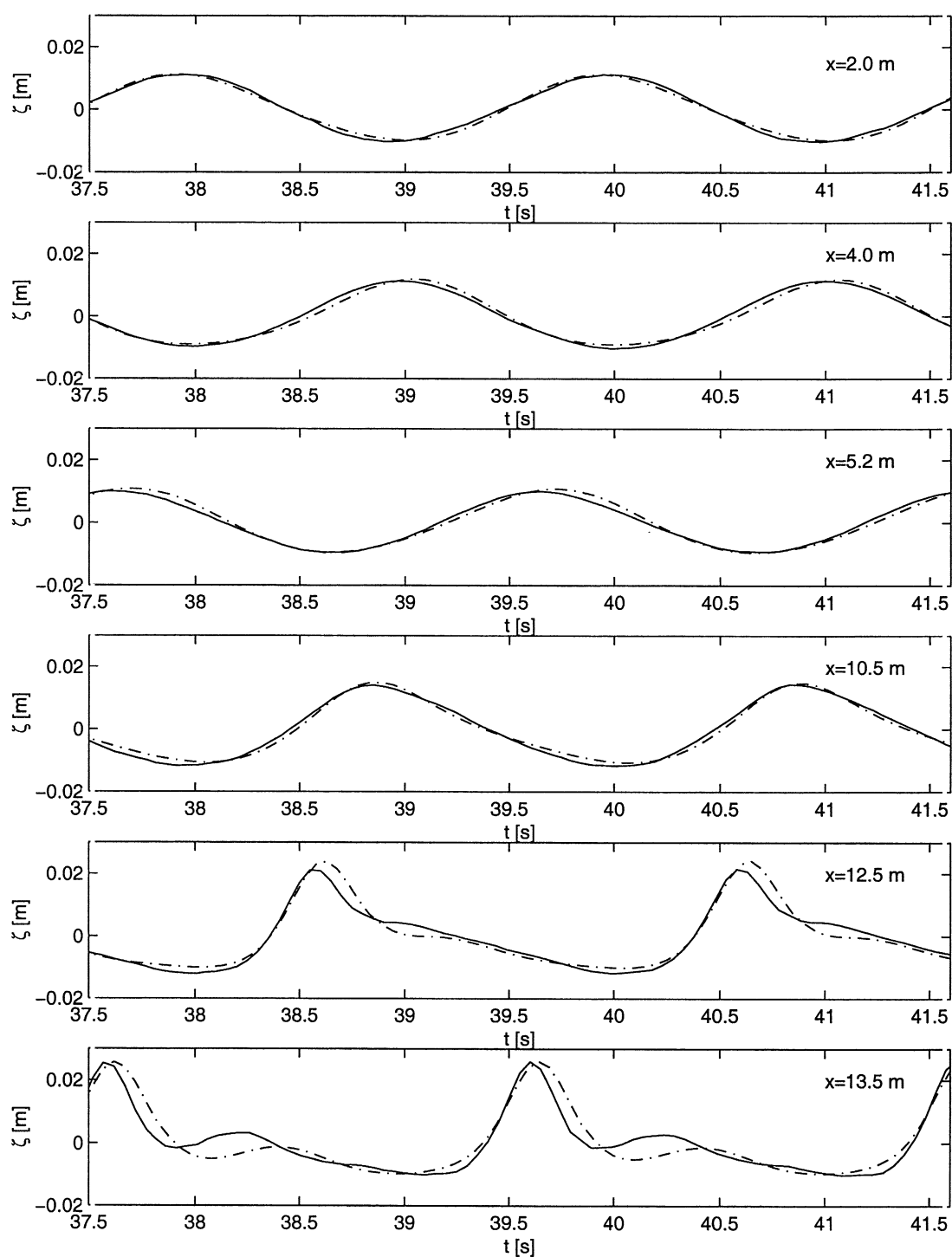


Figure F5a: Comparison of time series of surface elevation at stations 1-6 for measurement condition A (Dingemans, 1994) (—: measurements; - - - computations)

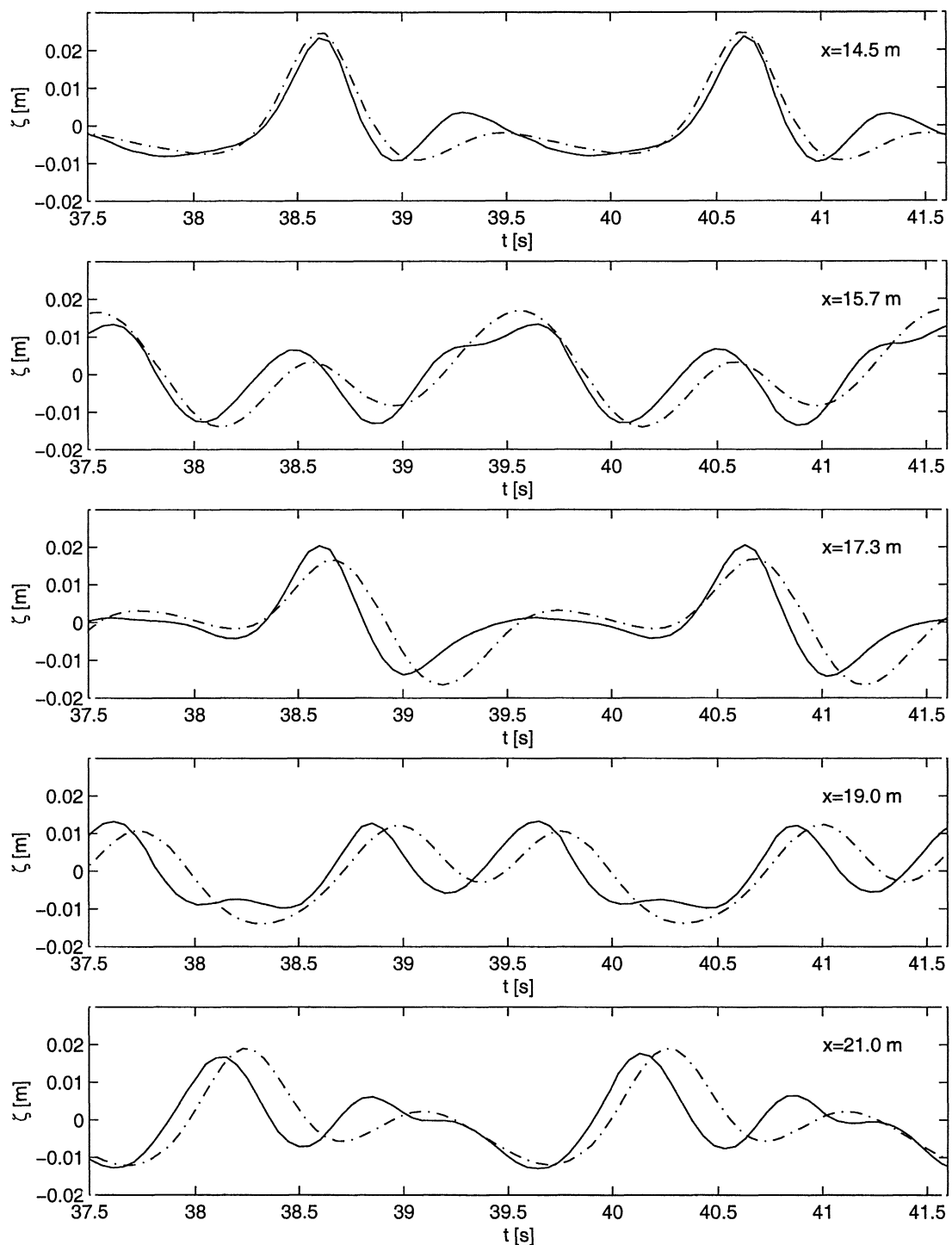


Figure F5b: Comparison of time series of surface elevation at stations 7-11 for measurement condition A (Dingemans, 1994) (—: measurements; - - - computations)

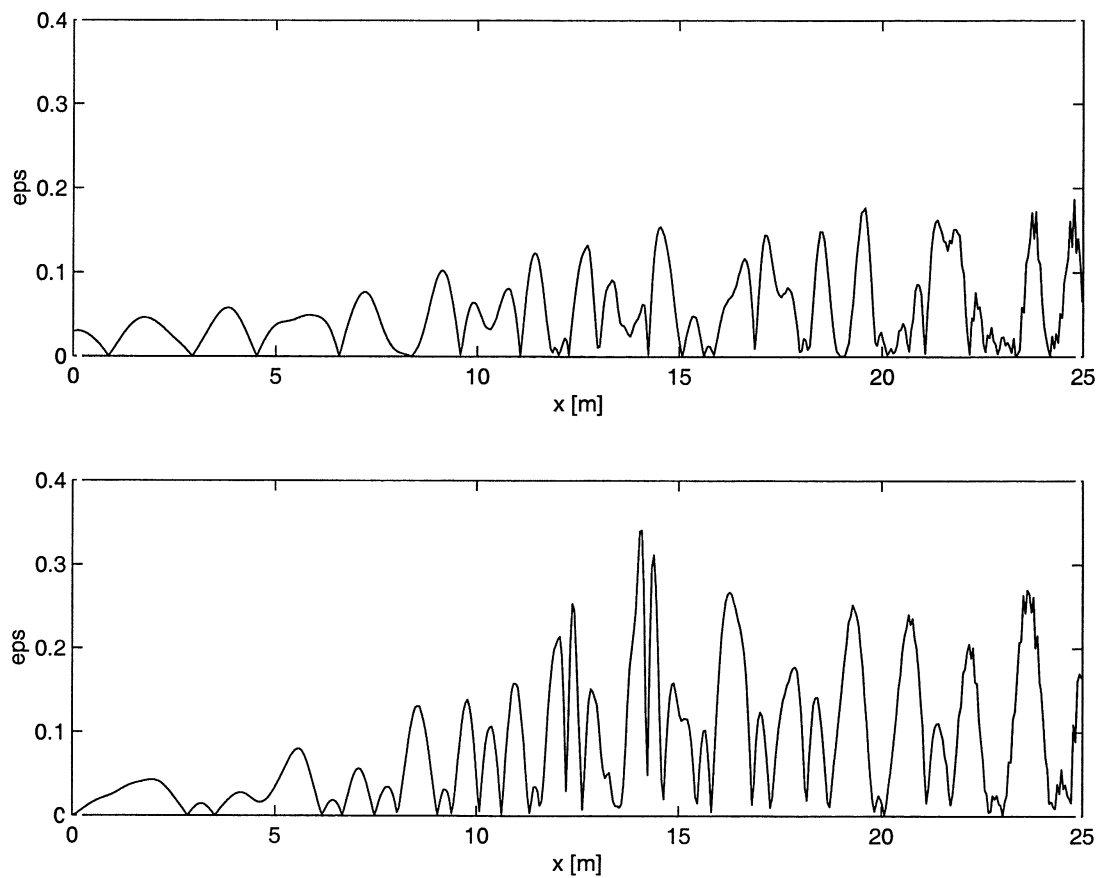


Figure F6: Reflection errors at $t_n = 50.5\text{s}$ obtained with present analysis (upper figure) and long wave assumption (lower figure)

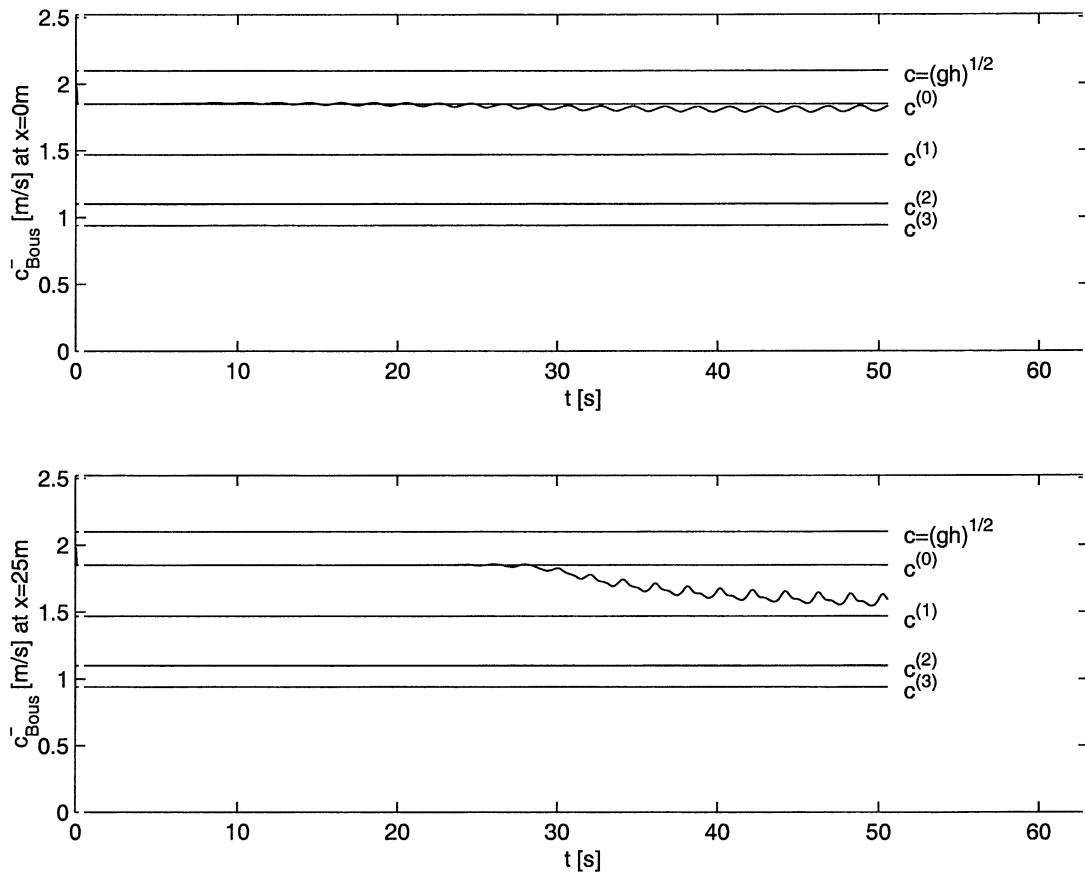


Figure F7: Computed values for \bar{c}_{Bous} at left and right boundary

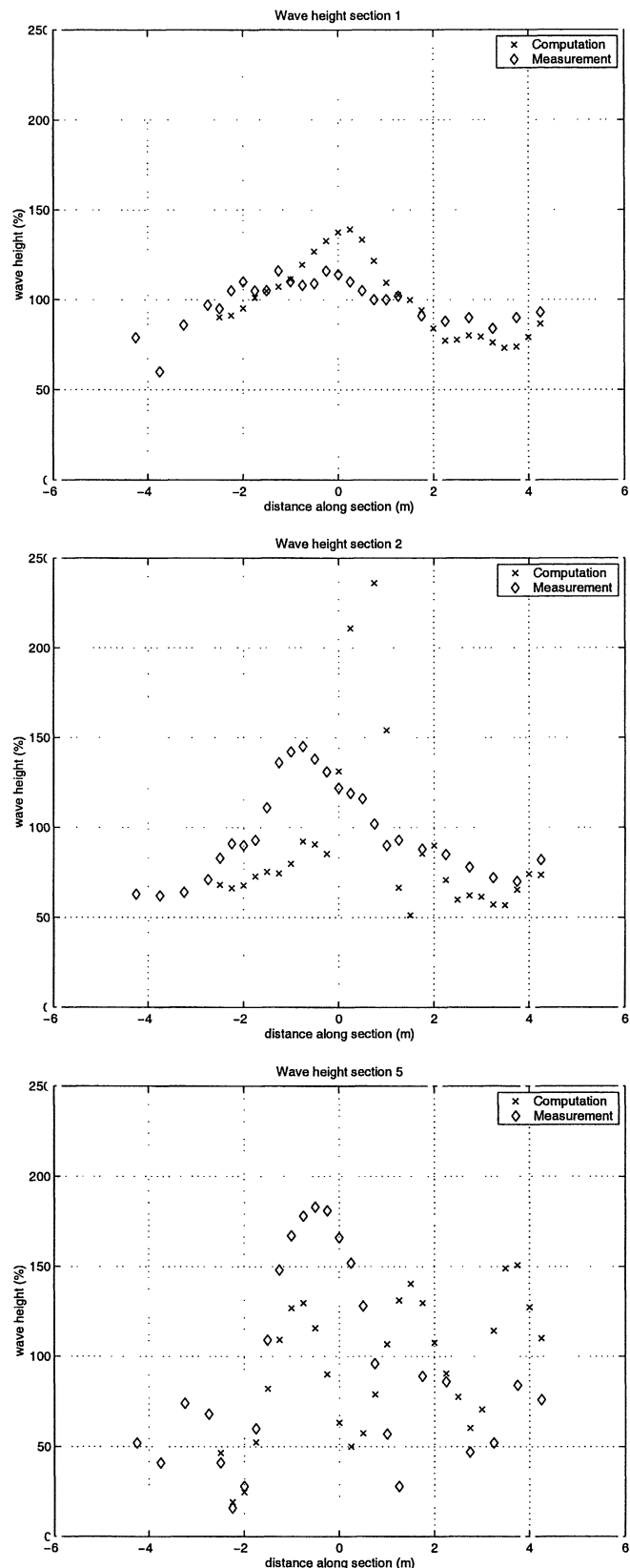


Figure F8a Comparison of numerical results (x) and experimental data (◊) for wave heights on measuring transects 1, 2 and 5 of Berkhoff et al. (1982)

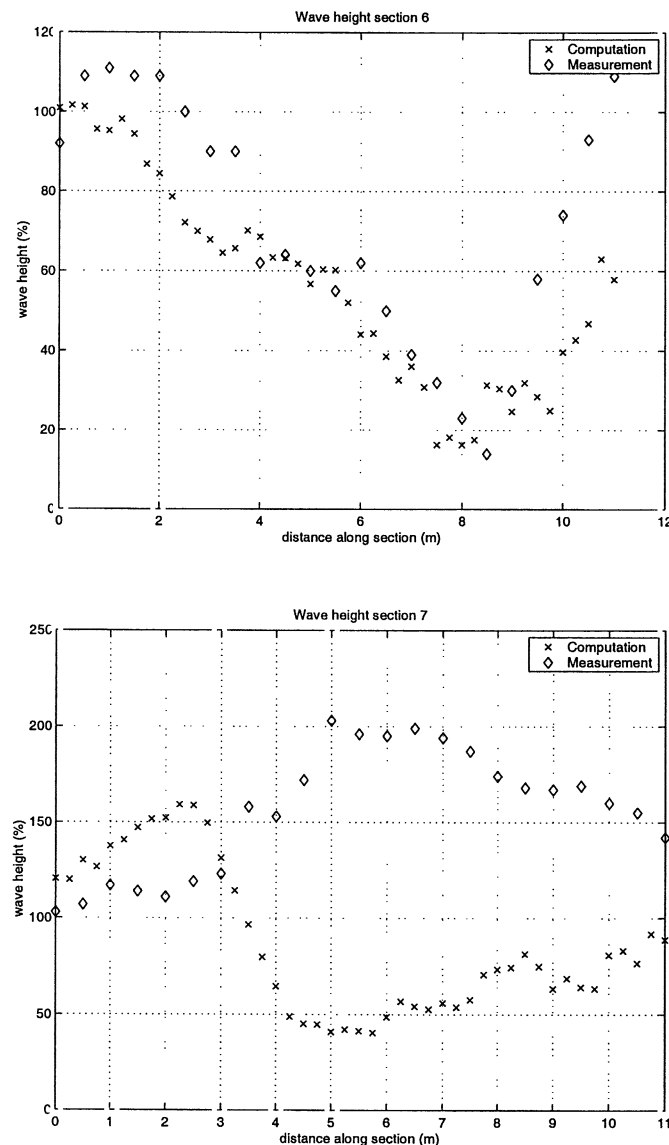


Figure F8b Comparison of numerical results (x) and experimental data (◊) for wave heights on measuring transects 6 and 7 of Berkhoff et al. (1982)